nature portfolio

Peer Review File

Highly Porous Metal-organic Framework Glass Design and Application for Gas Separation Membranes

Corresponding Author: Professor Thomas Bennett

This file contains all reviewer reports in order by version, followed by all author rebuttals in order by version.

Version 0:

Reviewer comments:

Reviewer #1

(Remarks to the Author)
This paper reports on two derivatives of previously studied ZIFs with the AFI and CAN topologies that can be transformed into porous melt-quenched glasses by partially replacing the original imidazolate linkers with benzimidazolates. The original ZIFs, which feature only imidazolate linkers, transform into dense ZIFs with zni topology when heated to high temperatures. However, the partial substitution with benzimidazolate prevents the formation of the zni phase, allowing the materials to melt at lower temperatures and transform into porous glasses upon cooling below the glass transition temperature.
The general strategy of linker exchange to obtain ZIF glasses has been reported in several studies, including by many of the authors. The finding that this strategy can also be applied to ZIFs with AFI and CAN topologies is a very valuable and important addition to the field. However, the novelty of this paper is somewhat limited, given that the melting of other highly porous ZIFs with LTA and SOD topologies has been previously shown (see for example https://doi.org/10.1038/s41467-018-07532-z and https://doi.org/10.1038/s41467-024-48703-5). Notably, the authors have prepared self-standing membranes of AFI ZIF using a pressing and remelting technique, demonstrating very good to excellent gas separation properties. Further insights into the origin of the improved permeance and selectivity of these glass membranes compared to the state of the art would provide valuable knowledge, certainly suitable for publication in Nature Communications.

Below are several questions, suggestions, and comments that should be addressed in a revised article:

1. Topological engineering to obtain porous ZIF glasses from highly porous ZIF crystals with compositions similar to those used here has been reported for ZIFs with LTA and SOD topologies (see references above). The authors should compare the porosity of their new ZIFs with these state-of-the-art glasses and not just with ZIF-62.

2. A recent study showed that the porosity of ZIF-62 glass diminishes when the sample is pressed or tempered at elevated temperature (https://doi.org/10.1038/s41563-023-01738-3). Since the glasses reported here are initially more porous but feature a composition identical to ZIF-62 derivatives, it is important to determine if the AFI ZIF glasses also densify when heated around the glass transition temperature for a few hours, particularly for potential membrane applications.

3. The structure of the CAN ZIF is not shown in the manuscript. Please introduce this structure, as readers may be unfamiliar with it. Additionally, compare the crystallographic porosities of AFI and CAN ZIFs with those of CAG, LTA, and SOD crystals. Are AFI and CAN topologies significantly more porous than SOD and LTA?

4. While potentially beyond the scope of the current work, it would be interesting to learn about the influence of benzimidazolate content on the thermal and glass-forming behavior. The chemical compositions used are similar to prototypical ZIF-62 glass formers. Was this intentional? Higher amounts of benzimidazolate might achieve higher porosity.

5. Are the N2 porosities of the Zn(Im)2 derivatives of AFI and CAN similar to those previously reported? Does the loss in porosity in AFI due to benzimidazolate inclusion align with expectations based on chemical composition? Why is the porosity of the benzimidazolate-containing CAN version significantly lower? The PXRD pattern intensities do not match the reported CAN structure well; is there a parasitic non-porous phase in the material which might explain the lower porosity?

6. The authors assign weak DSC signals to amorphization and melting. On what basis has this been done? What distinguishes an amorphous phase from a melt-quenched glass phase if the amorphous phase forms at the glass transition

temperature? Does the thermally amorphized phase exhibit a glass transition if reheated to 700 K?

7. The melting peaks in the DSC are very small. On what basis are these signals assigned to melting? Could the authors provide melting enthalpies? It might be better to record DSC scans of evacuated (guest-free) samples to avoid solvent evaporation obstructing important heat flow signals.

8. Why are the first upscans run at 20 K/min? Are the heat flow signatures for amorphization and melting so weak that they require high rates for observation?

9. Why does the AFI ZIF not feature hysteresis for N2 sorption but does for H2? Since H2 has a smaller kinetic diameter and the data were collected at the same temperature, this discrepancy needs clarification.

10. Comparing CO2 capacities of different glasses at 273 K and 1 bar does not provide reliable information on accessible porosity (see https://doi.org/10.1038/s41467-022-35372-5). Since only a very small fraction of the relative pressure scale is covered in this experiment, materials having narrow pores might adsorbed larger amounts of CO2 compared to ones that have larger pores (compare for example the CO2 uptake of crystalline ZIF-8 and ZIF-7 at that conditions). Measurements should be recorded at higher pressures or lower temperatures for reliable comparisons.

11. It is know that He penetrates in micropores in pycnometeic measurements. Hence, He pycnometric densities yield skeletal densities, ie. densities excluding the micropore volume. Since the He pycnometric density of AFI ZIF glass is very low, the presence of blocked and inaccessible porosity in the AFI ZIF glass may be suspected. This requires further explanation.

12. The term "defect-free" for the membranes needs clarification. Glasses typically have a lot of disorder and defects. Isn't a defect-free glass a crystal?

13. The AFI ZIF has been pressed to 10 MPa, a high pressure. It is unclear whether the crystalline material used for pressing was solvent-free or solvent-containing. The properties of the membrane may not be rationalised based on the gas sorption isotherms of the glasses prepared from powders without pressing. Hence, the structural integrity post-pressing should be confirmed by PXRD, and porosity post-pressing should be evaluated using CO2 gas sorption and compared to the data recorded for the glasses made from powders.

14. In TEM imaging, dark and bright spots in an amorphous sample do not naturally correspond to atom and pore positions. The incoherent electron scattering of amorphous structures makes it difficult to assign the observed interference pattern to a real-space atomic structure. Direct determination of micropore sizes and atom-atom distances of amorphous materials by TEM imaging is not possible. Unfortunately, such kind of analyses are regularly reported in the MOF glass literature.

15. The diffusivities measured by Knebel et al. using IR microscopy cannot be compared directly to the membrane diffusivities reported here.

16. All the crystallographic parameters in the Supplement should include estimated standard deviations.

17. The signal assignment in Fig. S4 is unclear. The sharp exothermic peak in the DSC trace is not assigned, while very weak signals are assigned to crystallization and melting. Melting and recrystallisation typically involve larger heat flow signatures. Reporting of enthalpies is highly encouraged.

18. All 1H NMR spectra should be shown in more detail, including a zoom into the aromatic region and the addition of integrals to the signals.

Reviewer #2

(Remarks to the Author)
The authors prepared two meltable MOFs, AFI-[Zn(Im)1.68(bIm)0.32] and CAN-[Zn(Im)1.73(bIm)0.27], with large 12-membered rings pores using both structure-directing agents and mixed organic ligands. The enhanced porosity carries over to the glass upon melt quenching, resulting in high H2, CO2 and CH4 adsorption capacities. Further, a free-standing agAFI-[Zn(Im)1.68(bIm)0.32] membrane was fabricated, showing very high gas permeance of around 104 GPU for CO2 and CO2/N2 selectivity of around 15. The research is valuable. However, some critical points need to be elaborated to provide a clearer understanding. The paper could be published after addressing the concerns raised below:

(1) The BET surface areas of AFI-[Zn(Im)1.68(bIm)0.32] (1015 m2/g) are basically same with that of AFI-[Zn(Im)2] (1103 m2/g). The result is different from normal cognition. Often, the N2 adsorption amounts would decrease with the increase content of bulky bIm ligand. Besides, whether the bIm content in the AFI-[Zn(Im)2-x(bIm)x] sample could be adjusted?

(2) The solubility coefficient (S) and diffusion coefficient (D) of membranes were measured by using constant volume-variable pressure method with pure gas (time-lag method). How about the pressure of the feed gas since the solubility coefficients are pressure related. Besides, it didn't give the N2 adsorption isotherm of agAFI-[Zn(Im)1.68(bIm)0.32] and agZIF-62 at the membrane test temperature. How did the authors obtain the N2 solubility coefficients?

(3) The membrane stability under high pressure is very important to the industrial application of membrane gas separation.

How about the effect of the transmembrane pressure on the gas separation stability of the self-supported glass membranes?

(4) The supported agZIF-62 membrane showed CO2/N2 selectivity higher than 30 (Fig. 6c), why the self-supported thicker agZIF-62 membrane in this paper showed mixed selectivity lower than 10?

(5) In line 281, the authors considered that the separation mechanism of agAFI-[Zn(Im)1.68(bIm)0.32] membrane was through molecular sieving. However, as can be seen from Table S4, the CH4/N2 diffusion selectivity was around 1 and the membrane performance was mainly attributed to the adsorption selectivity. The HR-TEM dark field images of agAFI-[Zn(Im)1.68(bIm)0.32] membrane also indicated that the transport channel is at the nanoscale (Fig. S14), which is difficult to achieve efficient molecular sieve separation.

Reviewer #3

(Remarks to the Author)
In this work, the authors reported the preparation of MOF glass membranes with large pore sizes for high-permanence gas separation. The results would be important for MOF and membrane materials in this hot field. However, several important issues should be addressed before Nature Communications considers accepting it.

1. Have the SDAs been removed before the glass conversion process? If not, what is the effect of SDAs on the pore structure of converted MOF glass?

2. Do the mixed ligands affect the melting point and MOF glass membrane preparation?

3. The mechanical stability test should be carried out on the membrane samples.

4. The pore size distribution of this work's MOF and MOF glass materials should be summarized in the main text.

5. Why do AFI-[Zn(Im)1.68(bIm)0.32] and CAN-[Zn(Im)1.73(bIm)0.27], both of which possess high porosity, exhibit significantly different pore structure after glass conversion? More discussion is needed.

6. Page 6, line 141-3, the authors stated, “The powder XRD patterns of .... (Fig.1b).” Please check the corresponding figure number here.

7. Please enlarge the font size in Fig 2e and 2f and pinpoint every TA, Tm, and Tg with arrows. Furthermore, on Page 10, line 242-5, the authors noted, "Moreover, the large solvent molecules used as SDAs in the synthesis ....that possibly decrease the decomposition temperature or increase the melting point of the resultant MOF crystals.” However, the Tm of the two materials reported in this work does not increase compared to ZIF-62. Since this study involves a variety of temperature values for different materials, it is recommended that the results be summarized in a table more clearly.

8. Some units for the X-axis in Fig 4 are wrong. Relative pressure units (e.g., P/P0) should be used instead of absolute pressure units when testing under critical conditions.

9. Supplementing the SEM images of membrane surface morphology in Fig 5 is suggested.

10. Page 11, line 277, the authors noted that “The gas permeance decreased with increasing the kinetic diameter of gas molecules.” However, the behavior of the three gases studied in this work generally does not follow this trend. Please expand on this to avoid any ambiguity.

11. The membrane thickness is several hundred micrometers, and the gas adsorption on the membrane materials is not very high, but the gas permeance is very high. More commentary and explanation should be provided on this point. Dead-end pores may be formed in the MOF glass membranes, reducing the effective membrane thickness.

Reviewer #4

(Remarks to the Author)
This manuscript reports the strategy of enhancing the porosity of MOF glasses by topological engineering of meltable crystalline ZIFs, which is novel and effective. The enhancement of gas separation performance of the ZIF glass membrane is very impressive. However, some issues need to be further discussed. Thus, I would recommend minor revision before acceptance.
1.Conduct additional experiments to validate the maximum bIm substitution ratios of AFI-[Zn(Im)1-x(bIm)x] and CAN-[Zn(Im)1-x(bIm)x] hybrids, including comprehensive characterization of their structural and pore properties.
2.The authors stated that the lower BET surface area of CAN-[Zn(Im)1.73(bIm)0.27] than CAN-[Zn(Im)2] was attributed to the degree of disorder. Conduct additional experiments to increase the BET value, the as-synthesized CAN-[Zn(Im)1.73(bIm)0.27] can be immersed in dry acetone.
3.Could the authors compare the porosity of AFI MOF before and after melt-quanching? Please also discuss the collapse process of pores in AFI MOF during melt-quanching. This is the key to validate the idea of this work.
4.The thickness of the membrane is about 200 μm. Could the authors discuss the prospect of practical applications of that

thick membrane?
5.The authors stated that the separation mechanism is molecular sieving. The kinetic diameter of CH4 is larger than N2. However, the membrane displays higher CH4 permeance than N2. Why?
6.Please explain the extremely higher gas diffusivity of the agAFI than agZIF-62.
7.The authors stated that the agAFI shows advantages in precise manipulation of porosity compared with agZIF-62 foam. Please explain more here.

Version 1:

Reviewer comments:

Reviewer #1

(Remarks to the Author)
The authors have done a very good job in revising their manuscript and addressing my questions. Several additional experiments have been conducted, and the new data and its discussion in the manuscript significantly enhance the overall quality of the work. In my opinion, this is a valuable contribution to the MOF glass field, and I support its publication in Nature Communications.

However, before publication, the authors need to address the following methodological issues:

1. The pressure axis of many H2, CO2, and CH4 sorption isotherms in the manuscript and supplementary information is erroneously labelled with p/p0. Here, p0 represents the saturation pressure (condensation pressure) of the respective gas at the isothermal measurement temperature. I believe most of these isotherms were measured at absolute pressures ranging from approximately 0 to 1 bar, not relative pressures of p/p0 = 1. For H2 at 77 K and for CO2 and CH4 at 273 K, p0 is substantially higher than 1 bar. Additionally, p0 is undefined for CO2 at 195 K since liquid CO2 (as present in the pores of the ZIF) does not exist in the phase diagram at this temperature. Except for the N2 sorption isotherm recorded at 77 K, the sorption data should be presented in absolute pressures. Furthermore, BET areas calculated from CO2 sorption isotherms recorded at 195 K must use a physically reasonable p0 value. An estimated p0 for the supercooled liquid phase of CO2, derived from the phase diagram, is approximately 1.9 bar, almost twice the value of p0 for the gas-solid transition of CO2. If a p0 of 1 bar is incorrectly assumed for analysis at 195 K, the BET surface areas are inaccurately calculated.

2. I previously requested the authors provide estimated standard deviations for their crystallographic data. While this has been done for some of the literature data discussed in the manuscript, the crystallographic parameters extracted from Pawley refinement should also be reported with standard deviations. The software used for profile fitting is not specified (please add this detail), but the package should be capable of providing standard deviations for lattice parameters, which must be included in the supplementary tables.

Reviewer #2

(Remarks to the Author)
I have carefully read the revised draft and the attachment, and the manuscript here can be accepted by NC at present。

Reviewer #3

(Remarks to the Author)
The authors have fully addressed the concerns, the manuscript in this version can be accepted.

Reviewer #4

(Remarks to the Author)
I recommend publishing the manuscript in its current state.

Version 2:

Reviewer comments:

Reviewer #1

(Remarks to the Author)
The authors have thoroughly revised their manuscript and successfully addressed all remaining issues. I would like to congratulate them on this outstanding work and look forward to its publication in Nature Communications.

RESPONSE TO REVIEWERS COMMENTS

Reviewer #1 (Remarks to the Author):

This paper reports on two derivatives of previously studied ZIFs with the AFI and CAN topologies that can be transformed into porous melt-quenched glasses by partially replacing the original imidazolate linkers with benzimidazolates. The original ZIFs, which feature only imidazolate linkers, transform into dense ZIFs with Zni topology when heated to high temperatures. However, the partial substitution with benzimidazolate prevents the formation of the Zni phase, allowing the materials to melt at lower temperatures and transform into porous glasses upon cooling below the glass transition temperature. The general strategy of linker exchange to obtain ZIF glasses has been reported in several studies, including by many of the authors. The finding that this strategy can also be applied to ZIFs with AFI and CAN topologies is a very valuable and important addition to the field. However, the novelty of this paper is somewhat limited, given that the melting of other highly porous ZIFs with LTA and SOD topologies has been previously shown (see for example https://doi.org/10.1038/s41467-018-07532-z and https://doi.org/10.1038/s41467-024-48703-5). Notably, the authors have prepared self-standing membranes of AFI ZIF using a pressing and remelting technique, demonstrating very good to excellent gas separation properties. Further insights into the origin of the improved permeance and selectivity of these glass membranes compared to the state of the art would provide valuable knowledge, certainly suitable for publication in Nature Communications. Below are several questions, suggestions, and comments that should be addressed in a revised article:

Comments 1. *Topological engineering to obtain porous ZIF glasses from highly porous ZIF crystals with compositions similar to those used here has been reported for ZIFs with LTA and SOD topologies (see references above). The authors should compare the porosity of their new ZIFs with these state-of-the-art glasses and not just with ZIF-62.* (https://doi.org/10.1038/s41467-018-07532-z and https://doi.org/10.1038/s41467-024-48703-5).

Response. We would like to express our gratitude for your careful review and valuable comments on our work.

A table of several ZIFs and corresponding structural diagrams have been added in the

revised manuscript. It is worth mentioning that due to the high-energy barrier of connector diffusion in open network structures, it has been reported that adding TIF-4[1] as a flux to ZIF-76 can help it melt, but ZIF-76 does not melt on its own. We will only supplement the analysis of pure phase meltable ZIF in the future. Add the following content to the article:

Comparison shows that the adsorption capacity and BET of a_gZIF-8 are both relatively high. From the analysis of crystal structure (Fig. S1, Table S1), although AFI and CAN have larger window apertures when the porosity difference is not significant, ZIF-8 has the lowest melting point (Table S1 and S5) and a lower degree of collapse during the melting process, retaining more pore channels.

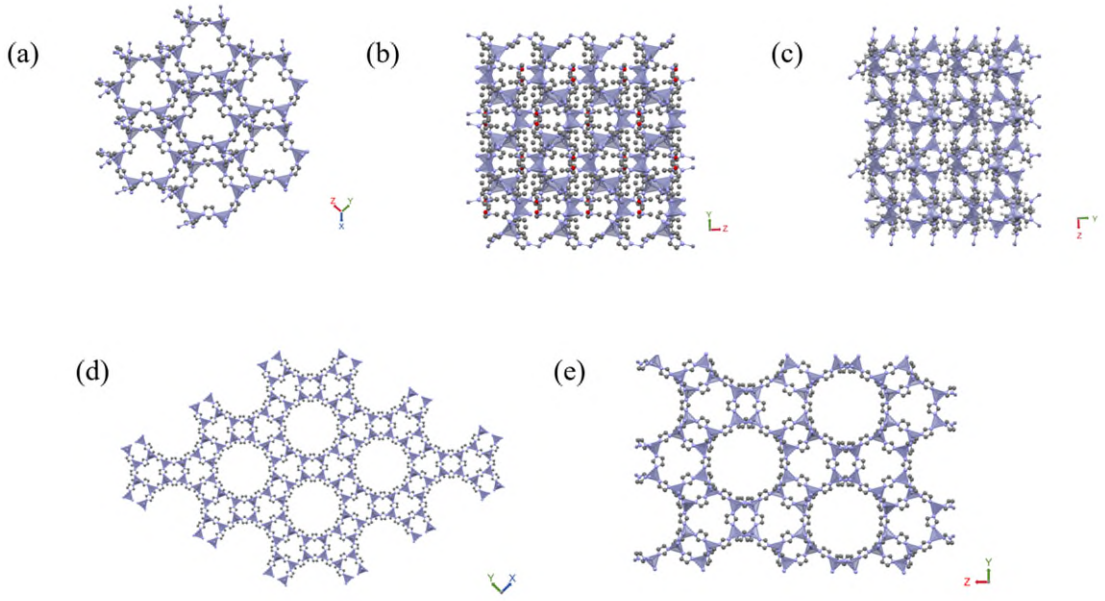

Fig. S1 ZIF structure diagrams (a) ZIF-8, (b) ZIF-62, (c) ZIF-4, (d) AFI-[$Zn(Im)_2$], and (e) CAN-[$Zn(Im)_2$][S1-S6]. The deep purple triangle represents Zn atoms, the purple sphere represents N atoms, and the gray sphere represents C atoms.

Table S1. Lists of representative ZIFs and their textural properties

Topology	Materials	Framework formula	Apertures Å	Ref
SOD	ZIF-8	$Zn(mIm)_2$	3.4	S2
CAG	ZIF-62	$Zn(Im)_{1.75}(bIm)_{0.25}$	1.4	S3, S4
CAG	ZIF-4	$Zn(Im)_2$	2.0	S5
AFI	AFI-[$Zn(Im)_2$]	$Zn(Im)_2$	20.0	S6
CAN	CAN-[$Zn(Im)_2$]	$Zn(Im)_2$	17.1	S6

[S1] Bumstead A M, Gómez M L R, Thorne M F, et al. Investigating the melting behaviour of polymorphic zeolitic imidazolate frameworks[J]. *Cryst. Eng. Comm*., 22(21) (2020) 3627-3637.
[S2] Lai Z. Development of ZIF-8 membranes: opportunities and challenges for commercial applications[J]. *Curr. Opin. Chem. Eng*., 20 (2018) 78-85.
[S3] Gandara-Loe J, Bueno-Perez R, Missyul A, Fairen-Jimenez D, Silvestre-Albero J. Molecular

Sieving Properties of Nanoporous Mixed-Linker ZIF-62: Associated Structural Changes upon Gas Adsorption Application. *ACS Appl. Nano. Mater.* **4**, (2021) 3519-3528.
[S4] Bennett T D, Yue Y, Li P, et al. Melt-quenched glasses of metal–organic frameworks. *J. Am. Chem. Soc*., 138(10) (2016) 3484-3492.
[S5] Anh Phan, Christian J. Doonan, Fernando J. Uribe-Romo, Carolyn B. Knobler, Michael O'Keeffe, Omar M. Yaghi, Synthesis, Structure, and Carbon Dioxide Capture Properties of Zeolitic Imidazolate Frameworks, *Acc. Chem. Res*. 43 (2010) 58-67.
[S6] Qi Shi, Wei-Jian Xu, Rui-Kang Huang, Wei-Xiong Zhang, Yang Li, Pengfei Wang, Fa-Nian Shi, Libo Li, Jinping Li, Jinxiang Dong, Zeolite CAN and AFI-Type Zeolitic Imidazolate Frameworks with Large 12-Membered Ring Pore Openings Synthesized Using Bulky Amides as Structure-Directing Agents, *J. Am. Chem. Soc*. 138 (2016) 16232-16235.

The pore volumes and pore size distributions of a_gAFI-[Zn(Im)$_{1.68}$(bIm)$_{0.32}$] and a_gCAN-[Zn(Im)$_{1.55}$(bIm)$_{0.45}$]were tested by CO_2 adsorption-desorption curves at 195 K, and the comparison was made with other MOF glasses in Table 1.

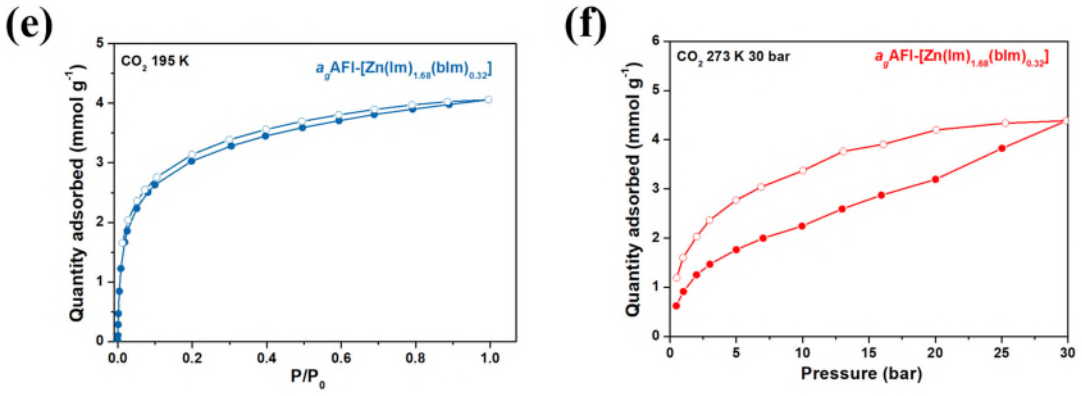

Fig. 4 Gas isotherms of a_gAFI-[Zn(Im)$_{1.68}$(bIm)$_{0.32}$] tested by (e) CO_2 at 195 K and (f) CO_2 at 273 K and 30 bar.

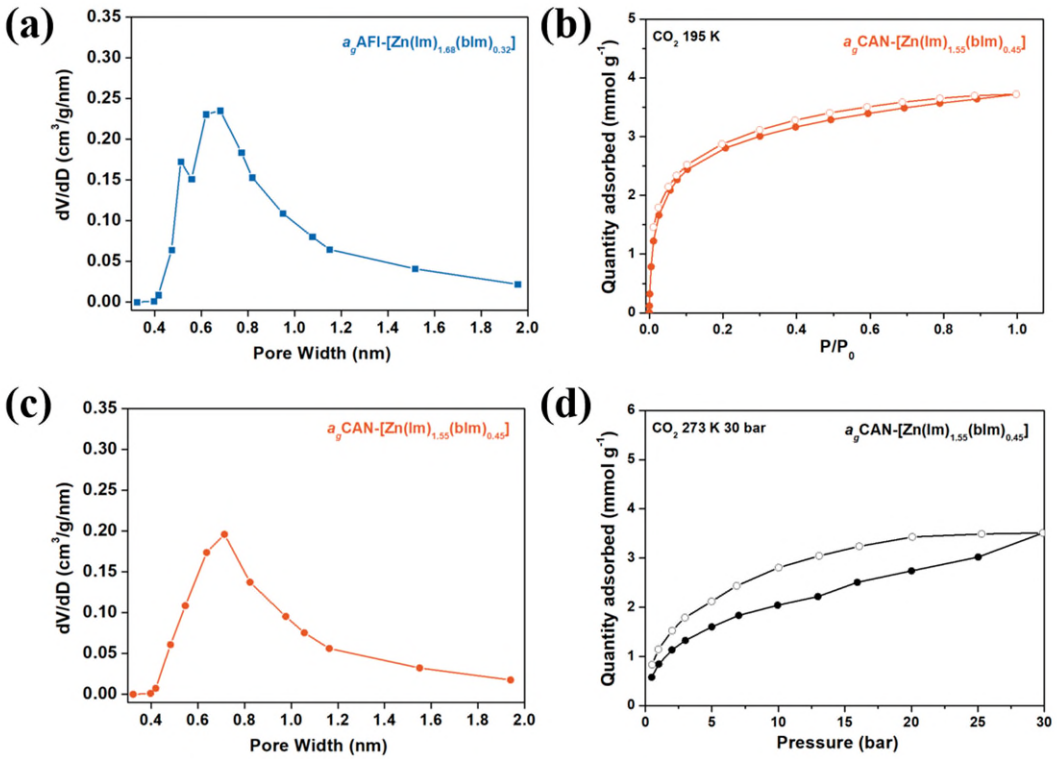

Fig. S19 (a) Pore size distribution of a_gAFI-[Zn(Im)$_{1.68}$(bIm)$_{0.32}$] obtained by CO_2 isotherms at 195 K. (b) CO_2 isotherms at 195 K, (c) pore size distribution, and (d) the high-pressure CO_2 adsorption at 273 K and 30 bar for a_gCAN-Zn(Im)$_{1.55}$(bIm)$_{0.45}$].

Tabel 1 Gas capacities, BET values, and pore volumes obtained by 195 K CO_2 isotherms.

Sample	Method	V_{ads} (cm^3/g)	n_{ads} (mmol/g)	S_{BET} (m^2/g)	V_{pore} (cm^3/g)	Ref.
a_gZIF-62	195 K CO_2	74.8	3.34	200	0.12	34
a_gTIF-4	195 K CO_2	76.2	3.4	204	0.12	34
a_gZIF-4	195 K CO_2	63.6	2.84	187	0.10	34
a_gZIF-67-mim$_{0.18}$im$_{0.68}$bim$_{0.14}$	195 K CO_2	118.5	5.3	316	0.18	35
a_gZIF-8-mim$_{0.15}$im$_{0.74}$bim$_{0.11}$	195 K CO_2	125.0	5.6	403	0.20	35
a_gCAN-bIm-[Zn(Im)$_{1.55}$(bIm)$_{0.45}$]	195 K CO_2	83.5	3.72	241	0.14	This work
a_gAFI-	195 K	91.0	4.06	285	0.16	This

$[Zn(Im)_{1.68}(bIm)_{0.32}]$	CO_2	work

Comments 2. *A recent study showed that the porosity of ZIF-62 glass diminishes when the sample is pressed or tempered at elevated temperature (https://doi.org/10.1038/s41563-023-01738-3). Since the glasses reported here are initially more porous but feature a composition identical to ZIF-62 derivatives, it is important to determine if the AFI ZIF glasses also densify when heated around the glass transition temperature for a few hours, particularly for potential membrane applications.*

Response.

In reported work (https://doi.org/10.1038/s41563-023-01738-3), ZIF-62 sample was heated to 450 °C under a nitrogen atmosphere and maintained at this temperature for 5 minutes. The insufficient duration of temperature during the preparation of ZIF-62 glass has resulted in inadequate collapse of the internal pores of ZIF-62 glass. Consequently, additional tempering will result in further collapse of the pores of ZIF-62 glass. Therefore, sufficient heating time will lead to more complete pore collapse of ZIF-62 glass.

In this work, the a_gAFI-$[Zn(Im)_{1.68}(bIm)_{0.32}]$ was heated at 705 K for 30 minutes. Furthermore, the a_gAFI-$[Zn(Im)_{1.68}(bIm)_{0.32}]$ was also heated around above the glass transition temperature (T_g=673 K) for 2 hours, resulting in the formation of the a_gAFI-$[Zn(Im)_{1.68}(bIm)_{0.32}]_T$. The CO_2 adsorption curves at 273 K indicates that the CO_2 adsorption capacity of a_gAFI-$[Zn(Im)_{1.68}(bIm)_{0.32}]_T$ exhibits a slight decrease, from 2.4 mmol/g to 2.3 mmol/g, in comparison to the CO_2 adsorption capacity of a_gAFI-$[Zn(Im)_{1.68}(bIm)_{0.32}]$. The slight reduction in CO_2 adsorption capacity is indicative of the complete collapse of the pores in the a_gAFI-$[Zn(Im)_{1.68}(bIm)_{0.32}]$ following the initial adequate heat treatment. Furthermore, the a_gAFI-$[Zn(Im)_{1.68}(bIm)_{0.32}]$ synthesized in this work is suitable for membrane separation applications, as it can be produced using a one-time heating and moulding process, which reduces energy loss caused by repeated heating. Additionally, the membrane displays good gas separation performance. The explanation has been added to the revised manuscript (lines 261-265, page 9) and highlighted in red.

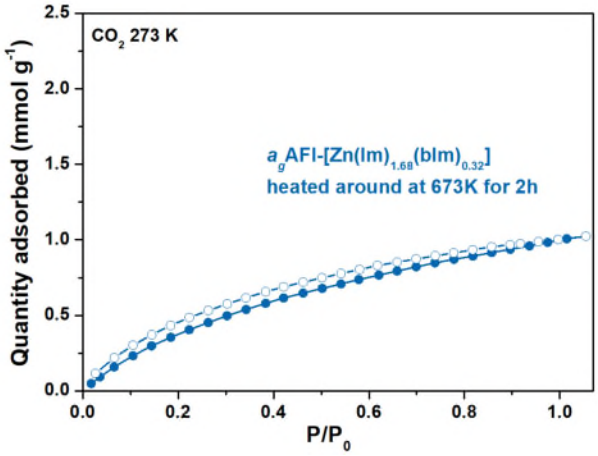

Fig. S21 the CO_2 adsorption isotherm of a_gAFI-$[Zn(Im)_{1.68}(bIm)_{0.32}]_T$ glass heated around at 673 K (above T_g) for 2h.

Comments 3. *The structure of the CAN ZIF is not shown in the manuscript. Please introduce this structure, as readers may be unfamiliar with it. Additionally, compare the crystallographic porosities of AFI and CAN ZIFs with those of CAG, LTA, and SOD crystals. Are AFI and CAN topologies significantly more porous than SOD and LTA?*

Response.

Due to the high-energy barrier of connector diffusion in open network structures, it has been reported that adding TIF-4[1] as a flux to ZIF-76 can help it melt, but ZIF-76 does not melt on its own. We will only supplement the analysis of pure phase meltable ZIF. The following content has been added in the revised article.

From the analysis of crystal structure (Fig. S1, Table S1), ZIFs with AFI and CAN topology shows larger window apertures than ZIFs with CAG and SOD topology.

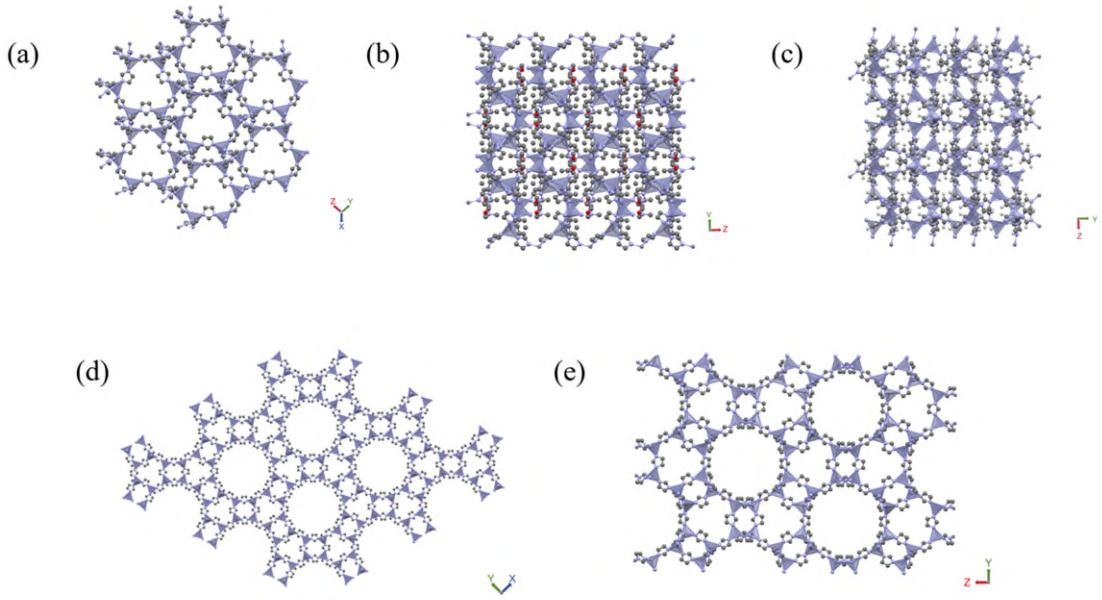

Fig. S1 ZIF structure diagrams (a) ZIF-8, (b) ZIF-62, (c) ZIF-4, (d) AFI-[$Zn(Im)_2$], and (e) CAN-[$Zn(Im)_2$][S1-S6]. The deep purple triangle represents Zn atoms, the purple sphere represents N atoms, and the gray sphere represents C atoms.

Table S1. Lists of representative ZIFs and their textural properties

Topology	Materials	Framework formula	Apertures Å	Ref
SOD	ZIF-8	$Zn(mIm)_2$	3.4	S2
CAG	ZIF-62	$Zn(Im)_{1.75}(bIm)_{0.25}$	1.4	S3, S4
CAG	ZIF-4	$Zn(Im)_2$	2.0	S5
AFI	AFI-$Zn(Im)_2$	$Zn(Im)_2$	20.0	S6
CAN	CAN-$Zn(Im)_2$	$Zn(Im)_2$	17.1	S6

[S1] Bumstead A M, Gómez M L R, Thorne M F, et al. Investigating the melting behaviour of polymorphic zeolitic imidazolate frameworks[J]. *Cryst. Eng. Comm*., 22(21) (2020) 3627-3637.
[S2] Lai Z. Development of ZIF-8 membranes: opportunities and challenges for commercial applications[J]. *Curr. Opin. Chem. Eng*., 20 (2018) 78-85.
[S3] Gandara-Loe J, Bueno-Perez R, Missyul A, Fairen-Jimenez D, Silvestre-Albero J. Molecular Sieving Properties of Nanoporous Mixed-Linker ZIF-62: Associated Structural Changes upon Gas Adsorption Application. *ACS Appl. Nano. Mater.* **4**, (2021) 3519-3528.
[S4] Bennett T D, Yue Y, Li P, et al. Melt-quenched glasses of metal–organic frameworks. *J. Am. Chem. Soc*., 138(10) (2016) 3484-3492.
[S5] Anh Phan, Christian J. Doonan, Fernando J. Uribe-Romo, Carolyn B. Knobler, Michael O'Keeffe, Omar M. Yaghi, Synthesis, Structure, and Carbon Dioxide Capture Properties of Zeolitic Imidazolate Frameworks, *Acc. Chem. Res*. 43 (2010) 58-67.
[S6] Qi Shi, Wei-Jian Xu, Rui-Kang Huang, Wei-Xiong Zhang, Yang Li, Pengfei Wang, Fa-Nian Shi, Libo Li, Jinping Li, Jinxiang Dong, Zeolite CAN and AFI-Type Zeolitic Imidazolate Frameworks with Large 12-Membered Ring Pore Openings Synthesized Using Bulky Amides as Structure-Directing Agents, *J. Am. Chem. Soc*. 138 (2016) 16232-16235.

Comments 4. *While potentially beyond the scope of the current work, it would be interesting to learn about the influence of benzimidazolate content on the thermal and glass-forming behavior. The chemical compositions used are similar to prototypical ZIF-62 glass formers. Was this intentional? Higher amounts of benzimidazolate might*

achieve higher porosity.

Response.

This is indeed an urgent issue that needs to be considered at present, and relevant work is already underway. Further research will be conducted in the next article. The explanation has been added in the revised manuscript (lines 147-157, page 6).

The effects of bIm content on the performance of ZIF-62[27] and ZIF-8[32] have been reported. Henke et.al[27] found that the bIm linker partially occupies two of the four available imidazole salt positions in the ZIF-62 structure. By reducing the ratio of Im and bIm, the T_m of ZIF-62 can be reduced from 703 K to 643 K. The pore size distribution indicates that during the melting and formation of a_gZIF-62, small cavities (with a diameter of approximately 3.5 Å) completely disappear, but medium-sized cavities (with a diameter of 5-6 Å) are significantly preserved, and even new larger cavities (with a diameter of 8 Å) are formed. In previous studies[32, 33], bIm was used to replace one of the three mIm joints in ZIF-8. As the content of bIm increased, the pore size significantly decreased, the pore size distribution narrowed, and the thermal stability also decreased.

These works indicate that the content of bIm effectively affects the properties of MOF and MOF glass, and related research will be conducted in the future.

27. Frentzel-Beyme L, Kloss M, Kolodzeiski P, Pallach R, Henke S. Meltable Mixed-Linker Zeolitic Imidazolate Frameworks and Their Microporous Glasses: From Melting Point Engineering to Selective Hydrocarbon Sorption. *J Am Chem Soc* **141**, 12362-12371 (2019).
32. Krokidas P, et al. On the efficient separation of gas mixtures with the mixed-linker zeolitic-imidazolate framework-7-8. *ACS Appl. Mater. Interfaces* **10** 39631-39644 (2018).
33. Thompson JA, et al. Hybrid zeolitic imidazolate frameworks: controlling framework porosity and functionality by mixed-linker synthesis. *Chem*. *Mater*. **24**, 1930-1936 (2012).

Comments 5. *Are the N_2 porosities of the $Zn(Im)_2$ derivatives of AFI and CAN similar to those previously reported? Does the loss in porosity in AFI due to benzimidazolate inclusion align with expectations based on chemical composition? Why is the porosity of the benzimidazolate-containing CAN version significantly lower? The PXRD pattern intensities do not match the reported CAN structure well; is there a parasitic non-porous phase in the material which might explain the lower porosity?*

Response. The explanation has been added in the revised manuscript (lines 169-172, page 6), marked in red.

As shown in Fig. S3, we tested the BET at 77 N_2 of the newly synthesized AFI-[$Zn(Im)_2$]

and CAN-[$Zn(Im)_2$]. The results showed that the N_2 porosities values of AFI-[$Zn(Im)_2$] and CAN-[$Zn(Im)_2$] were similar to those previously reported, at 1155 cm^2 and 1033 cm^2, respectively. The N_2 adsorption amounts decreases after adding bulky bIm ligand in the framework, for example, the specific surface area decreases from 1155 m^2/g to 1073 m^2/g for AFI-[$Zn(Im)_2$] and AFI-[$Zn(Im)_{1.68}(bIm)_{0.32}$], from 1033 m^2/g to 603 m^2/g for CAN-[$Zn(Im)_2$] and CAN-[$Zn(Im)_{1.73}(bIm)_{0.27}$].

The effects of bIm content on the performance of ZIF-62[27] and ZIF-8[32] have been reported. Henke et.al[27] found that the bIm linker partially occupies two of the four available imidazole salt positions in the ZIF-62 structure. By reducing the ratio of Im and bIm, the T_m of ZIF-62 can be reduced from 703 K to 643 K. The pore size distribution indicates that during the melting and formation of a_gZIF-62, small cavities (with a diameter of approximately 3.5 Å) completely disappear, but medium-sized cavities (with a diameter of 5-6 Å) are significantly preserved, and even new larger cavities (with a diameter of 8 Å) are formed. In previous studies[32, 33], bIm was used to replace one of the three mIm joints in ZIF-8. As the content of bIm increased, the pore size significantly decreased, the pore size distribution narrowed, and the thermal stability also decreased.

These works indicate that the content of bIm effectively affects the properties of MOF and MOF glass, and related research will be conducted in the future.

27. Frentzel-Beyme L, Kloss M, Kolodzeiski P, Pallach R, Henke S. Meltable Mixed-Linker Zeolitic Imidazolate Frameworks and Their Microporous Glasses: From Melting Point Engineering to Selective Hydrocarbon Sorption. *J Am Chem Soc* **141**, 12362-12371 (2019).
32. Krokidas P, et al. On the efficient separation of gas mixtures with the mixed-linker zeolitic-imidazolate framework-7-8. *ACS Appl. Mater. Interfaces* **10** 39631-39644 (2018).
33. Thompson JA, et al. Hybrid zeolitic imidazolate frameworks: controlling framework porosity and functionality by mixed-linker synthesis. *Chem*. *Mater*. **24**, 1930-1936 (2012).

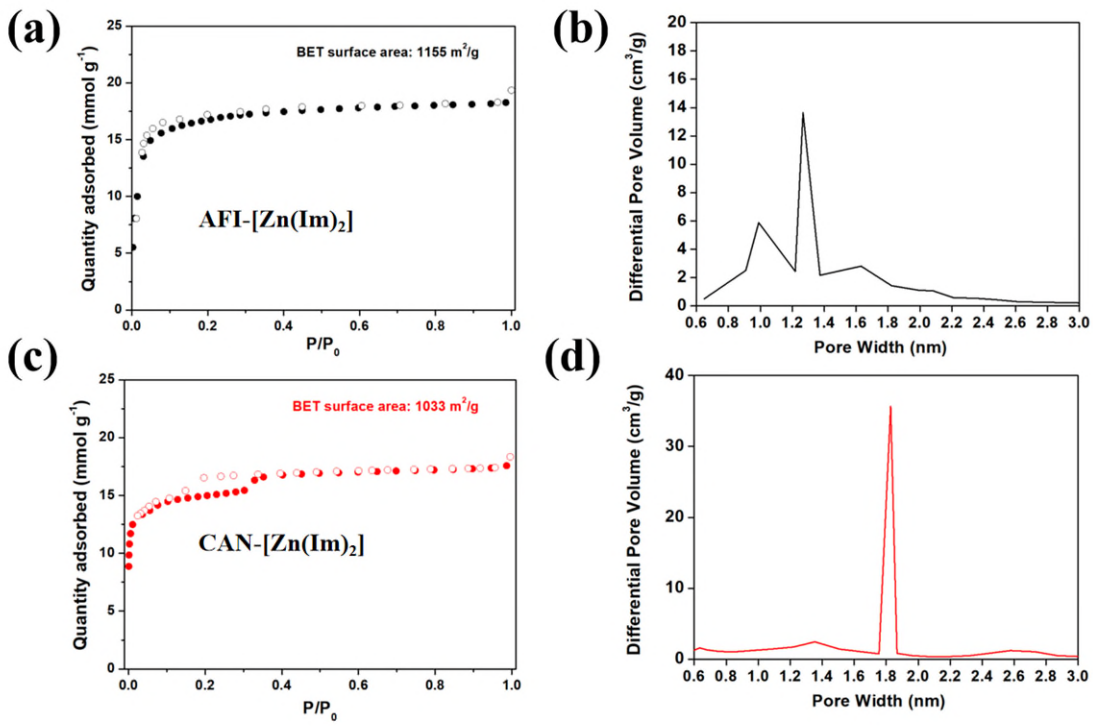

Fig. S3 N_2 isotherms at 77 K of (a) AFI-[$Zn(Im)_2$] and (c) CAN-[$Zn(Im)_2$]; Pore size distribution of (b) AFI-[$Zn(Im)_2$] and (d) CAN-[$Zn(Im)_2$].

In addition, the lower BET surface area of CAN-[$Zn(Im)_{1.73}(bIm)_{0.27}$] than CAN-[$Zn(Im)_2$] (Supplementary Fig. 3) is attributed to that the synthesized CAN-[$Zn(Im)_{1.73}(bIm)_{0.27}$] has low crystallinity, resulting in low porosity of the crystals. The explanation has been added in the revised manuscript (lines 172-175, page 6), marked in red.

The XRD patterns of CAN-[$Zn(Im)_2$] were enlarged in the experiment and found to be in general agreement with the simulated pattern, and the results have been confirmed by Powley refinement (Fig S2 and Table S2).

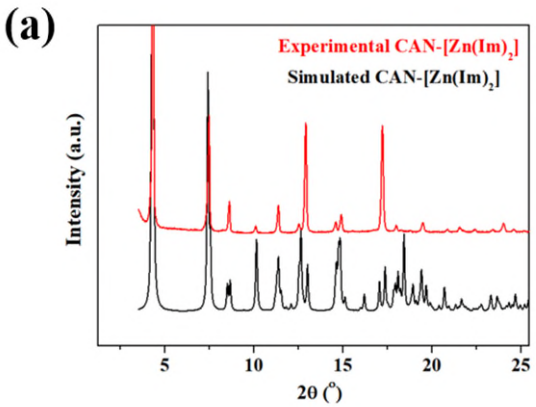

Fig. R1. The enlarged XRD patterns of CAN-[$Zn(Im)_2$].

Comments 6. *The authors assign weak DSC signals to amorphization and melting. On what basis has this been done? What distinguishes an amorphous phase from a melt-quenched glass phase if the amorphous phase forms at the glass transition temperature? Does the thermally amorphized phase exhibit a glass transition if reheated to 700 K?*

Response.

Initially, the amorphous temperature T_A was reached through the first round of DSC scanning, followed by the second and third rounds of scanning, as illustrated in the Supplementary Fig. 17. Following the initial amorphization process, AFI-[$Zn(Im)_{1.68}(bIm)_{0.32}$] exhibited both melting and glass transition characteristics.

Furthermore, AFI-[$Zn(Im)_{1.68}(bIm)_{0.32}$] was subjected to heating above the T_A (650 K) for the three scans. As illustrated in Fig. S14, it was evident that heating to the amorphous temperature was insufficient to induce melting and glass transition of AFI-[$Zn(Im)_{1.68}(bIm)_{0.32}$].

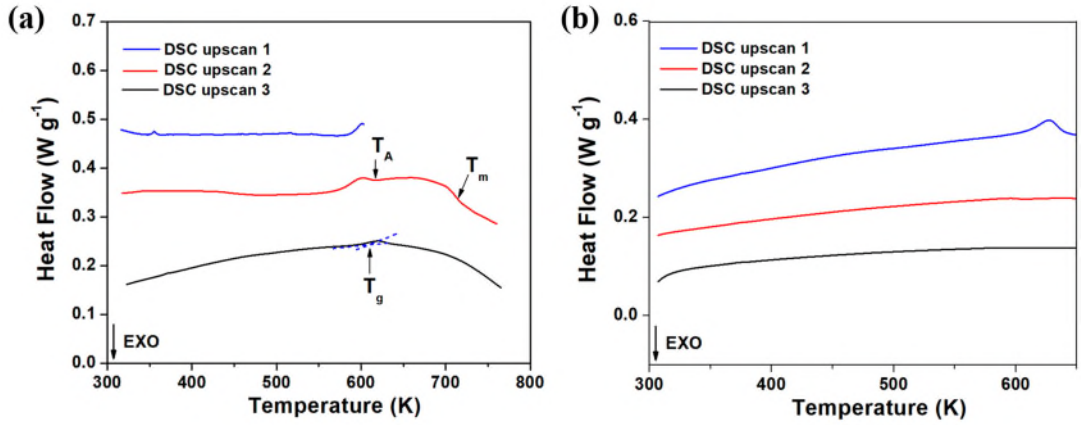

Fig. S14 DSC curves of AFI-[$Zn(Im)_{1.68}(bIm)_{0.32}$]. (a) heat up to T_A for the first scan, (b) heat up to T_A for the three scans.

Comments 7. *The melting peaks in the DSC are very small. On what basis are these signals assigned to melting? Could the authors provide melting enthalpies? It might be better to record DSC scans of evacuated (guest-free) samples to avoid solvent evaporation obstructing important heat flow signals.*

Response.

Following the removal of the guest (as shown in TGA result), the AFI-[$Zn(Im)_{1.68}(bIm)_{0.32}$] was tested at a heating rate of 10 K/min, as shown in DSC curve of Fig. S12. The melting peak of AFI was relatively small, with an endothermic peak

appearing around 711 K, corresponding to the melting phenomenon. The initial DSC scan revealed that the ΔH_m value of the AFI-[$Zn(Im)_{1.68}(bIm)_{0.32}$] was 0.52 KJ/mol, which was listed in Table S5.

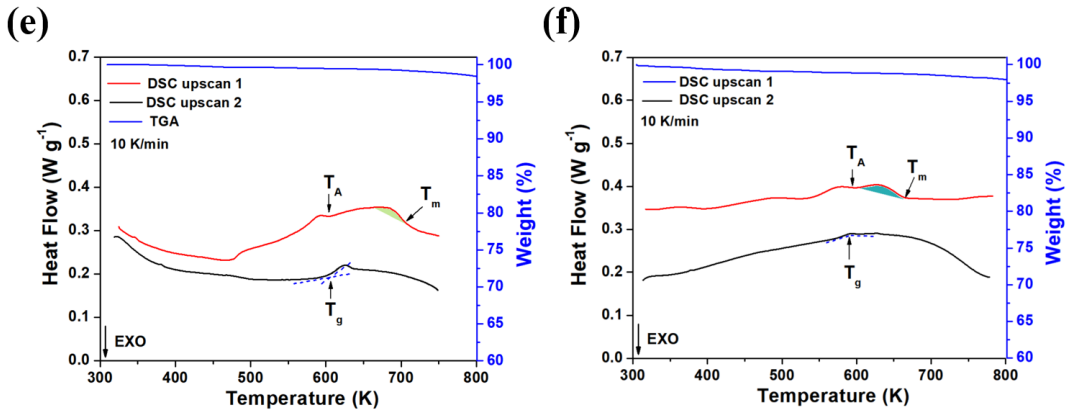

Fig. 2 TGA and DSC curves for AFI-[$Zn(Im)_{1.68}(bIm)_{0.32}$] and CAN-[$Zn(Im)_{1.73}(bIm)_{0.27}$] (the light green and blue shaded region highlights the integrated area for the determination of ΔH_m).

Table S5. Summary of the phase transition enthalpies obtained from the DSC data.

Material	Composition	T_m (K)	T_g (K)	ΔH_m (KJ/mol)	Ref.
ZIF-62	$Zn(Im)_{1.75}(bIm)_{0.25}$	708	604	2.92	S7
ZIF-4	$Zn(Im)_2$	852	-	11.46	S8
TIF-4	$Zn(Im)_{1.68}(mbIm)_{0.32}$	709	611	2.69	S8
ZIF-zni		858	-	11.88	S8
ZIF-UC-5		701	-	-	S9
ZIF-8-$mIm_{0.15}Im_{0.74}bIm_{0.11}$	$Zn(mIm)_{0.15}(Im)_{0.74}(bIm)_{0.11}$	641	-	0.66	S10
AFI	$Zn(Im)_{1.68}(bIm)_{0.32}$	711	607	0.52	This work
CAN	$Zn(Im)_{1.73}(bIm)_{0.27}$	670	591	0.50	This work

Comments 8. *Why are the first upscans run at 20 K/min? Are the heat flow signatures for amorphization and melting so weak that they require high rates for observation?*

Response. We would like to express our gratitude for your careful review and valuable comments on our work.

Moreover, DSC testing of AFI-[$Zn(Im)_{1.68}(bIm)_{0.32}$] and CAN-[$Zn(Im)_{1.73}(bIm)_{0.27}$] were evaluated at varying heating rates (10 K, 20 K, 30 K), the T_A, T_m, and T_g were

marked in Fig. S12 and Fig. S13. Both AFI-[Zn(Im)$_{1.68}$(bIm)$_{0.32}$] and CAN-[Zn(Im)$_{1.73}$(bIm)$_{0.27}$] displayed the characteristics of both melting and glass transition.

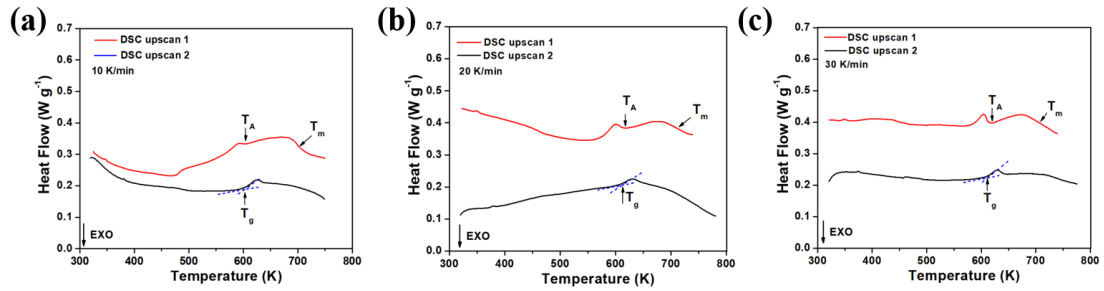

Fig. S12 DSC curves of AFI-[Zn(Im)$_{1.68}$(bIm)$_{0.32}$] at varying heating rates (a) 10 K, (b) 20 K, and (c) 30 K.

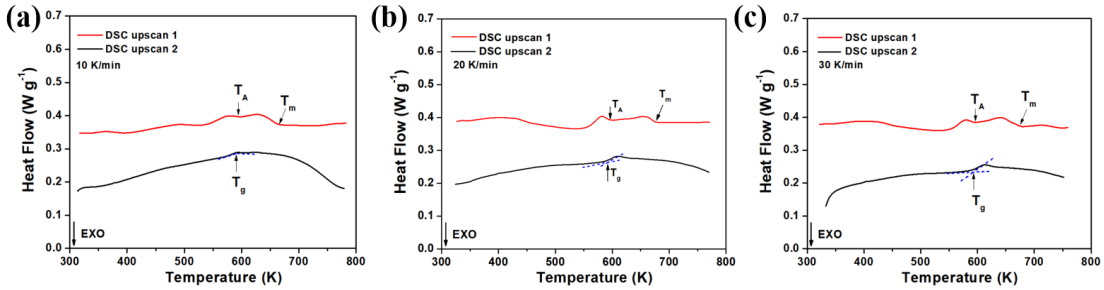

Fig. S13 DSC curves of CAN-[Zn(Im)$_{1.73}$(bIm)$_{0.27}$] at varying heating rates (a) 10 K, (b) 20 K, and (c) 30 K.

Comments 9. *Why does the AFI ZIF not feature hysteresis for N_2 sorption but does for H_2? Since H_2 has a smaller kinetic diameter and the data were collected at the same temperature, this discrepancy needs clarification.*

Response.

At 77K, H_2 molecules can form stronger interactions via van der Waals forces, weak chemical adsorption, or by binding to metal nodes and open metal sites within the MOF structure. These interactions may cause H_2 to become more tightly trapped during desorption, requiring greater energy or more time to release. Significant hysteresis during H_2 desorption has been reported in studies on MOF glass materials, such as a_gZIF-62 (*Nat. Mater.*, 2019, 18, 370-376). These studies confirmed the strong interaction between H_2 molecules and ZIF glasses. In contrast, N_2 primarily undergoes monolayer physical adsorption, which involves lower adsorption energy, allowing it to desorb more quickly at 77 K without displaying the pronounced hysteresis observed with H_2. Furthermore, in the aforementioned studies on MOF glass materials, low N_2

adsorption was reported, and no desorption hysteresis was observed, such as a_gZIF-8-mIm$_{0.15}$Im$_{0.74}$bIm$_{0.11}$ (*Nat. Commun.*, 2024, **15**, 4420) and a_gZIF-62 (*Nat. Mater.*, 2019, 18, 370-376). This suggests that N_2 molecules are either prevented from diffusing into the pores or, in cases where a small amount is adsorbed at 77 K, they desorb rapidly due to their size and weaker interactions with MOF glasses. The following has been modified and added in the revised manuscript (lines 243-247, page 9):

"No hysteresis was observed for N_2, indicating that N_2 molecules desorb rapidly due to their weaker interactions with a_gAFI-[Zn(Im)$_{1.68}$(bIm)$_{0.32}$], resulting in the absence of a hysteresis effect during N_2 desorption, similar case has been reported for a_gZIF-8-mIm$_{0.15}$Im$_{0.74}$bIm$_{0.11}$[35]."

Comments 10. *Comparing CO_2 capacities of different glasses at 273 K and 1 bar does not provide reliable information on accessible porosity (see https://doi.org/10.1038/s41467-022-35372-5). Since only a very small fraction of the relative pressure scale is covered in this experiment, materials having narrow pores might adsorbed larger amounts of CO_2 compared to ones that have larger pores (compare for example the CO_2 uptake of crystalline ZIF-8 and ZIF-7 at that conditions). Measurements should be recorded at higher pressures or lower temperatures for reliable comparisons.*

Response.

The CO_2 adsorption capacity of a_gAFI-[Zn(Im)$_{1.68}$(bIm)$_{0.32}$] and a_gCAN-[Zn(Im)$_{1.55}$(bIm)$_{0.45}$] was tested at higher pressures (273 K, 30 bar) and lower temperatures (195 K), respectively. As shown in Fig. 4(f), the high-pressure CO_2 gas adsorption at 273 K and 30 bar demonstrated the enhanced CO_2 adsorption capacity and pore continuity of a_gAFI-[Zn(Im)$_{1.68}$(bIm)$_{0.32}$]. This explanation has been added to Fig. 4 and revised manuscript (lines 253-255, page 9), marked in red.

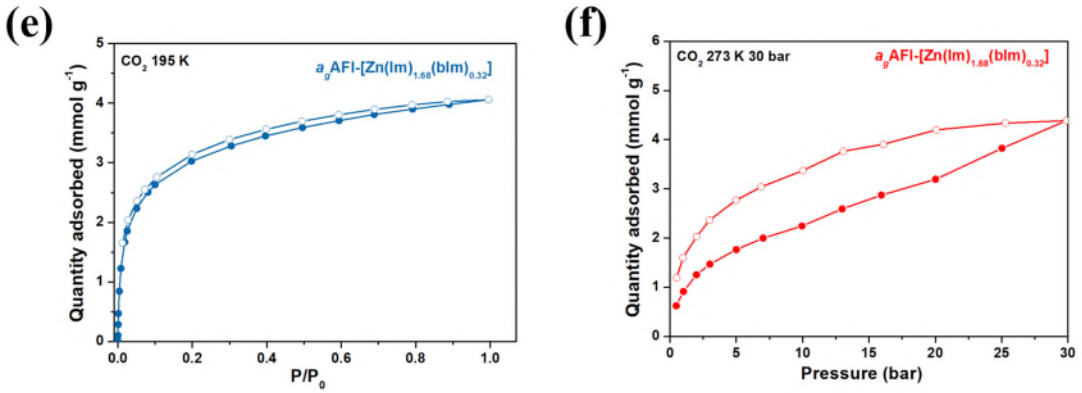

Fig. 4 Gas isotherms of a_gAFI-[Zn(Im)$_{1.68}$(bIm)$_{0.32}$] tested by (e) CO_2 at 195 K and (f) CO_2 at 273 K and 30 bar.

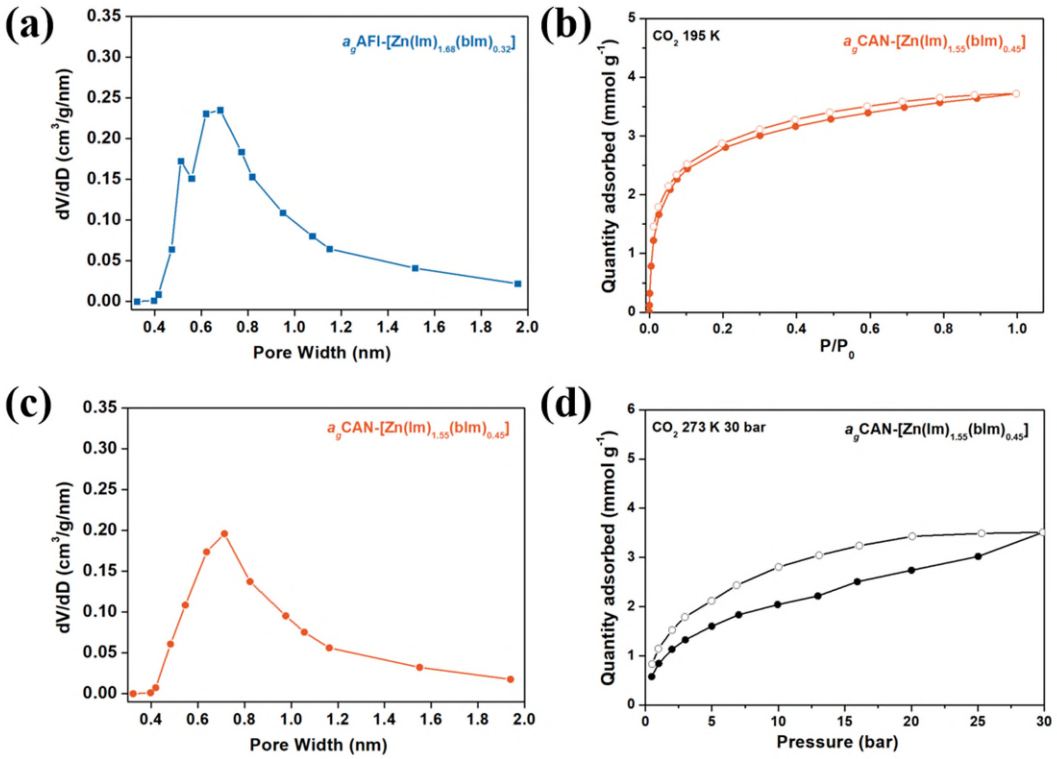

Fig. S19 (a) Pore size distribution of a_gAFI-[Zn(Im)$_{1.68}$(bIm)$_{0.32}$] obtained by CO_2 isotherms at 195 K. (b) CO_2 isotherms at 195 K, (c) pore size distribution, and (d) the high-pressure CO_2 adsorption at 273 K and 30 bar for a_gCAN-Zn(Im)$_{1.55}$(bIm)$_{0.45}$].

Comments 11. *It is know that He penetrates in micropores in pycnometeic measurements. Hence, He pycnometric densities yield skeletal densities, ie. densities excluding the micropore volume. Since the He pycnometric density of AFI ZIF glass is very low, the presence of blocked and inaccessible porosity in the AFI ZIF glass may be suspected. This requires further explanation.*

Response.

Moreover, the low density of a_gAFI-[Zn(Im)$_{1.68}$(bIm)$_{0.32}$] possibly indicates the presence of a multitude of blocked or inaccessible pores. During the transformation from crystal to glass, the collapse of the pore structure results in the formation of varying degrees of pore channels. Furthermore, it is unavoidable that some pores will become obstructed, preventing He from entering and resulting in a reduction in the He pycnometric density.

The explanation has been added to the revised manuscript (lines 276-281, page 10-11) and highlighted in red.

Comments 12. *The term "defect-free" for the membranes needs clarification. Glasses typically have a lot of disorder and defects. Isn't a defect-free glass a crystal?*

Response.

In order to avoid the ambiguous description, we have deleted the term "defect-free" in the revised manuscript.

In fact, the term ″defect-free″ is too broad and we have changed it to ″no obvious defects in membrane surface observed by SEM″, as shown in Fig. 5.

We used ″defect-free″ to describe the macroscopic morphology of the glass membrane, and the surface of the membrane observed by SEM is uniform and without obvious macroscopic defects, which does not mean that it has a perfectly ordered structure like a MOF crystal.

Fig. 5 The SEM images of the membrane surface (a) 10 μm, (b) 1 μm, and (c) 400 nm.

Comments 13. *The AFI ZIF has been pressed to 10 MPa, a high pressure. It is unclear whether the crystalline material used for pressing was solvent-free or solvent-containing. The properties of the membrane may not be rationalised based on the gas sorption isotherms of the glasses prepared from powders without pressing. Hence, the structural integrity post-pressing should be confirmed by PXRD, and porosity post-pressing should be evaluated using CO_2 gas sorption and compared to the data recorded for the glasses made from powders.*

Response.

Firstly, the TGA results shown in Fig. S20 indicated that AFI-$[Zn(Im)_{1.68}(bIm)_{0.32}]$ crystals did not exhibit significant solvent loss. This suggests that the activated AFI-$[Zn(Im)_{1.68}(bIm)_{0.32}]$ did not contain solvent. Secondly, XRD patterns of AFI-$[Zn(Im)_{1.68}(bIm)_{0.32}]$ after pressing showed a notable reduction in diffraction peak intensity. Thirdly, the AFI-$[Zn(Im)_{1.68}(bIm)_{0.32}]$ with post-pressing demonstrated a notable reduction in CO_2 adsorption capacity at 273K. The reduction in crystallinity

and adsorption capacity can be attributed to that the integrity of the crystal structure was damaged by the additional mechanical pressure. As shown in Fig. S20, following the melting and quenching process, both pre-pressing and post-pressing a_gAFI-[Zn(Im)$_{1.68}$(bIm)$_{0.32}$] exhibited an almost identical CO_2 adsorption capacity. Although mechanical pressure slightly damages the porous structure of AFI-[Zn(Im)$_{1.68}$(bIm)$_{0.32}$] crystals, it has almost no effects on the adsorption capacity of the melt-quenching glass. After being transformed into a glass state through melt-quenching, no significant difference in adsorption capacity was observed between the two. The explanation has been added to the revised manuscript (lines 253-261, page 9) and highlighted in red.

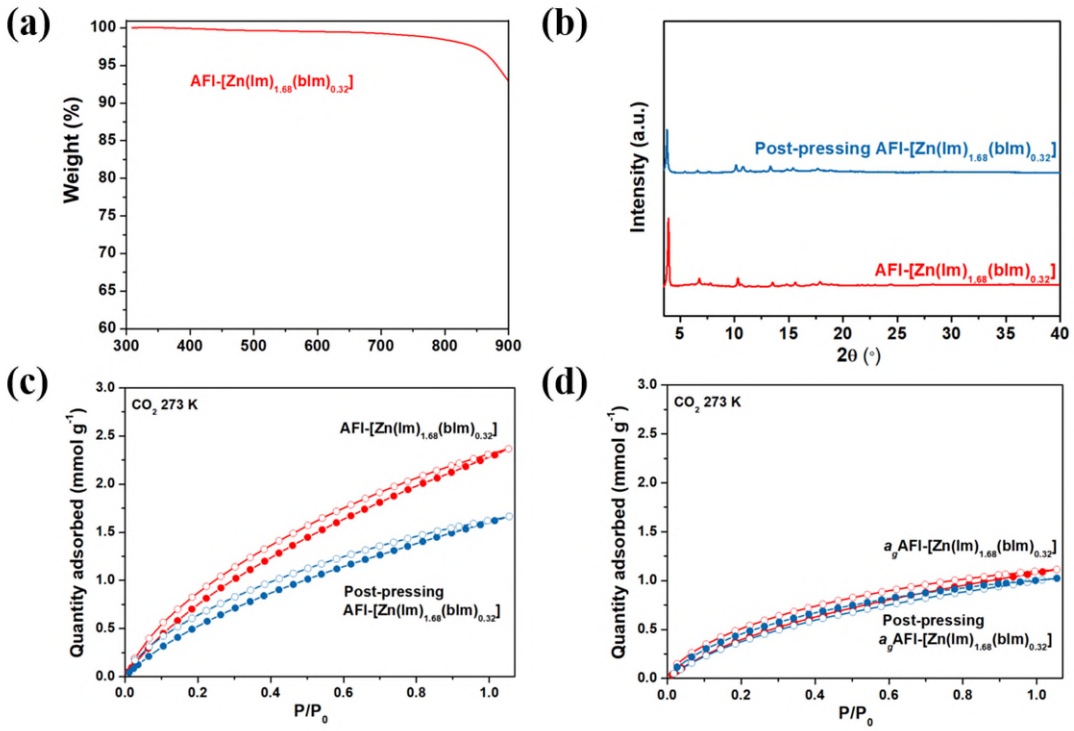

Fig. S20 (a) TGA result of AFI-[Zn(Im)$_{1.68}$(bIm)$_{0.32}$] with solvent-free, (b) XRD patterns of post-pressing of AFI-[Zn(Im)$_{1.68}$(bIm)$_{0.32}$], (c) CO_2 adsorption at 273 K for AFI-[Zn(Im)$_{1.68}$(bIm)$_{0.32}$] and post-pressing AFI-[Zn(Im)$_{1.68}$(bIm)$_{0.32}$], (d) CO_2 adsorption at 273 K for a_gAFI-[Zn(Im)$_{1.68}$(bIm)$_{0.32}$] and post-pressing a_gAFI-[Zn(Im)$_{1.68}$(bIm)$_{0.32}$].

Comments 14. *In TEM imaging, dark and bright spots in an amorphous sample do not naturally correspond to atom and pore positions. The incoherent electron scattering of amorphous structures makes it difficult to assign the observed interference pattern to a real-space atomic structure. Direct determination of micropore sizes and atom-atom distances of amorphous materials by TEM imaging is not possible. Unfortunately, such*

kind of analyses are regularly reported in the MOF glass literature.

Response.

We agree with your views on these images.

Nevertheless, many MOF glass literature have reported the utilization of HR-TEM for the observation of atomic and pore positions in amorphous samples, which may be attributed to the inherent difficulty in measuring the atomic-level structure of amorphous samples.

We have revised the description of the testing results for a_gAFI-[Zn(Im)$_{1.68}$(bIm)$_{0.32}$] using HR-TEM in the revised manuscript. The microstructure of a_gAFI-[Zn(Im)$_{1.68}$(bIm)$_{0.32}$] was observed to exhibit slight looseness, and the packing density was decreased when analyzed using HR-TEM.

"The large pores are partially preserved in the melt-quenched glass, named a_gAFI-[Zn(Im)$_{1.68}$(bIm)$_{0.32}$]." Furthermore, the enhanced adsorption capacity and pore continuity of the a_gAFI-[Zn(Im)$_{1.68}$(bIm)$_{0.32}$] were demonstrated through high-pressure CO_2 gas adsorption.

The explanation has been added to the revised manuscript (lines 317-319, page 12) and highlighted in red.

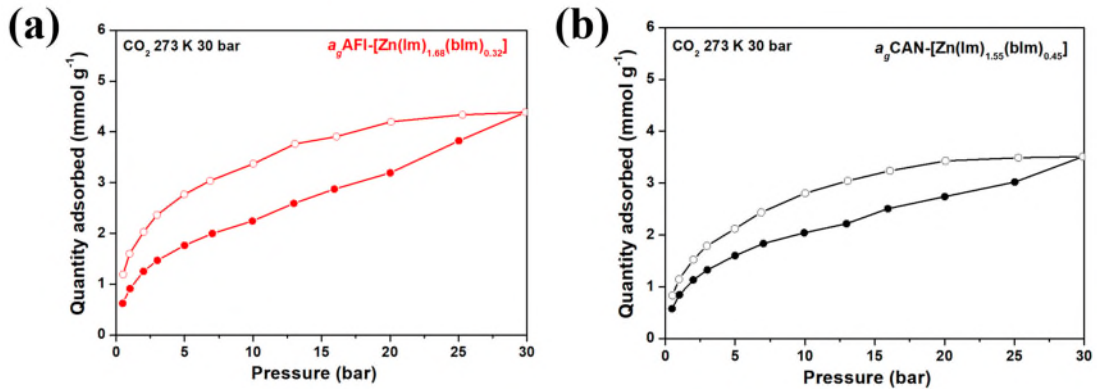

Fig. R3 the high-pressure CO_2 gas adsorption at 273 K and 30 bar (a) a_gAFI-[Zn(Im)$_{1.68}$(bIm)$_{0.32}$] and (b) a_gCAN-[Zn(Im)$_{1.55}$(bIm)$_{0.45}$].

Comments 15. *The diffusivities measured by Knebel et al. using IR microscopy cannot be compared directly to the membrane diffusivities reported here.*

Response. We would like to express our gratitude for your careful review and valuable comments on our work.

In reported work, Knebel et al. used an infrared microscope (Infrasil, Starna; cell inner diameter, 19 mm, cell height, 5 mm) to measure the diffusivities of gas molecules. The

concentration of gas molecules over time was then calculated by measuring the characteristic peak area of gas molecules in IR absorption spectra. The assessment of gas diffusivities in this work is conducted using the constant-volume variable-pressure time-lag method. However, the underlying principles of this approach and the method of Knebel et al. are not aligned, rendering direct comparisons between the two unreliable.

This explanation has already been revised to page 16, lines 411-415 of the revised manuscript, marked in red.

Comments 16. *All the crystallographic parameters in the Supplement should include estimated standard deviations.*

Response. The estimated standard deviations have been added in the Tables for CAN-[$Zn(Im)_2$] that are provided in the Cif file. The other estimated standard deviations were not provided either in the Cif file or refinement results.

Table S2 Lattice parameters of AFI-[$Zn(Im)_2$] and CAN-[$Zn(Im)_2$] obtained from reported cif files and Pawley refinement.

	Space group	**a (Å)**	**b (Å)**	**c (Å)**	**α (º)**	**β (º)**	**γ (º)**	**Ref.**
AFI-[$Zn(Im)_2$]	P6/MCC	26.4372	26.4372	16.6315	90	90	90	Cif
AFI-[$Zn(Im)_2$]	P6/MCC	26.2854	26.2854	16.2425	90	90	90	This work
CAN-[$Zn(Im)_2$]	Pnma	9.6256(8)	23.436(2)	41.593(3)	90	90	90	Cif
CAN-[$Zn(Im)_2$]	Pnma	9.93504	19.91213	39.20607	90	90	90	This work

Table S4 Lattice parameters of MOFs obtained from reported cif files and Pawley refinement.

	Space group	**a (Å)**	**b (Å)**	**c (Å)**	**α (º)**	**β (º)**	**γ (º)**	**Ref.**
AFI-[$Zn(Im)_2$]	P6/MCC	26.4372	26.4372	16.6315	90	90	90	Cif
AFI-[$Zn(Im)_{1.68}$(bI	P6/MCC	26.1382	26.1382	16.6051	90	90	90	This wor

m)$_{0.32}$]								k
CAN-[Zn(Im)$_2$]	Pnma	9.6256(8)	23.436(2)	41.593(3)	90	90	90	Cif
CAN-[Zn(Im)$_{1.73}$(bIm)$_{0.27}$]	Pnma	9.6234	23.540	41.205	90	90	90	This work

Comments 17. *The signal assignment in Fig. S4 is unclear. The sharp exothermic peak in the DSC trace is not assigned, while very weak signals are assigned to crystallization and melting. Melting and recrystallisation typically involve larger heat flow signatures. Reporting of enthalpies is highly encouraged.*

Response.

Following the removal of the guest, the CAN-[Zn(Im)$_2$] was tested at a heating rate of 10 K/min, as shown in DSC curve of Fig. S5. The initial DSC scan revealed that the ΔH_m value of the CAN-[Zn(Im)$_2$] was 18.4 KJ/mol.

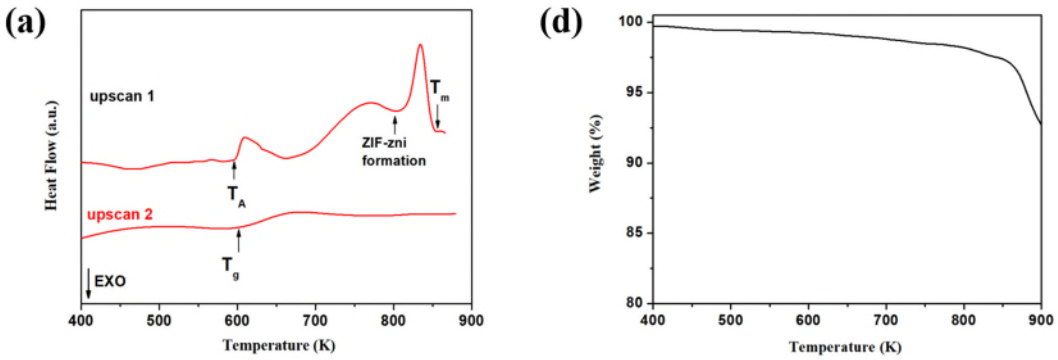

Fig. S5 (a) Enthalpic responses of CAN-[Zn(Im)$_2$] under Ar. and (d) TGA curve of CAN-[Zn(Im)$_2$] measured under Ar.

Comments 18. *All ^{1}H NMR spectra should be shown in more detail, including a zoom into the aromatic region and the addition of integrals to the signals.*

Response.

All ^{1}H NMR spectra, including the amplification of aromatic regions and integration into the signal, have been added in the supplementary materials.

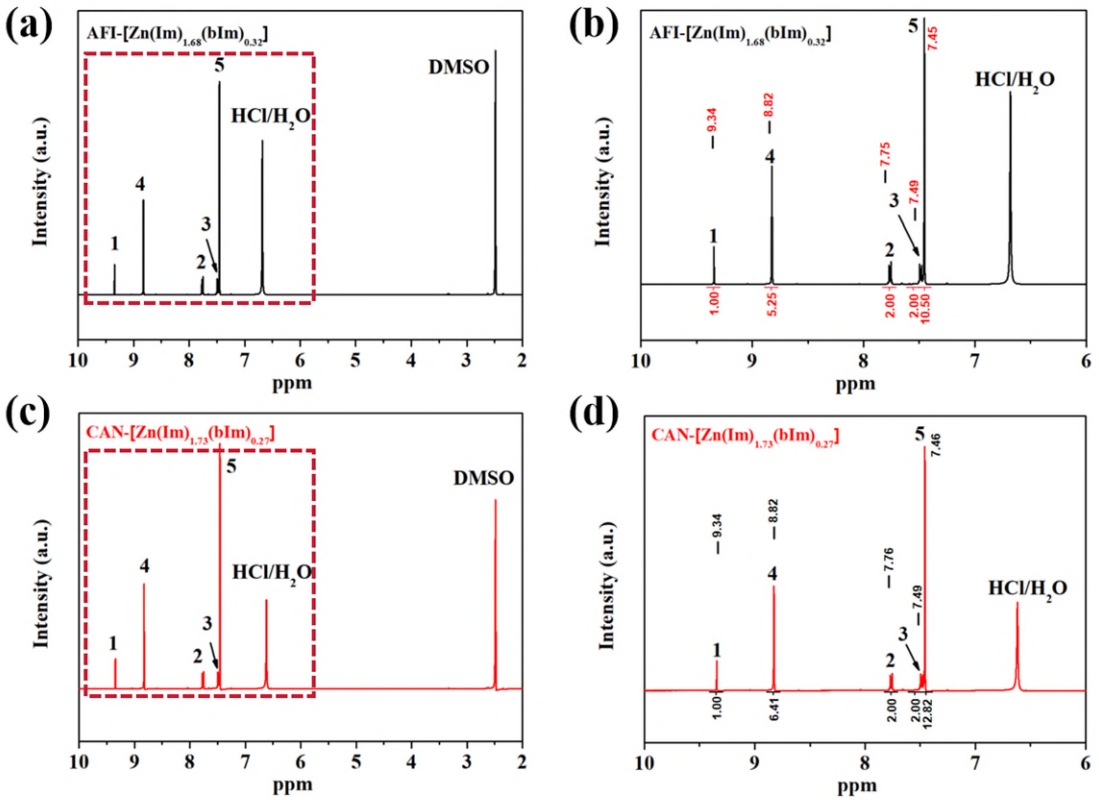

Fig. S8 ^{1}H NMR and Enlarged aromatic region for (a, b) AFI-[Zn(Im)$_{1.68}$(bIm)$_{0.32}$] and (c, d) CAN-[Zn(Im)$_{1.73}$(bIm)$_{0.27}$].

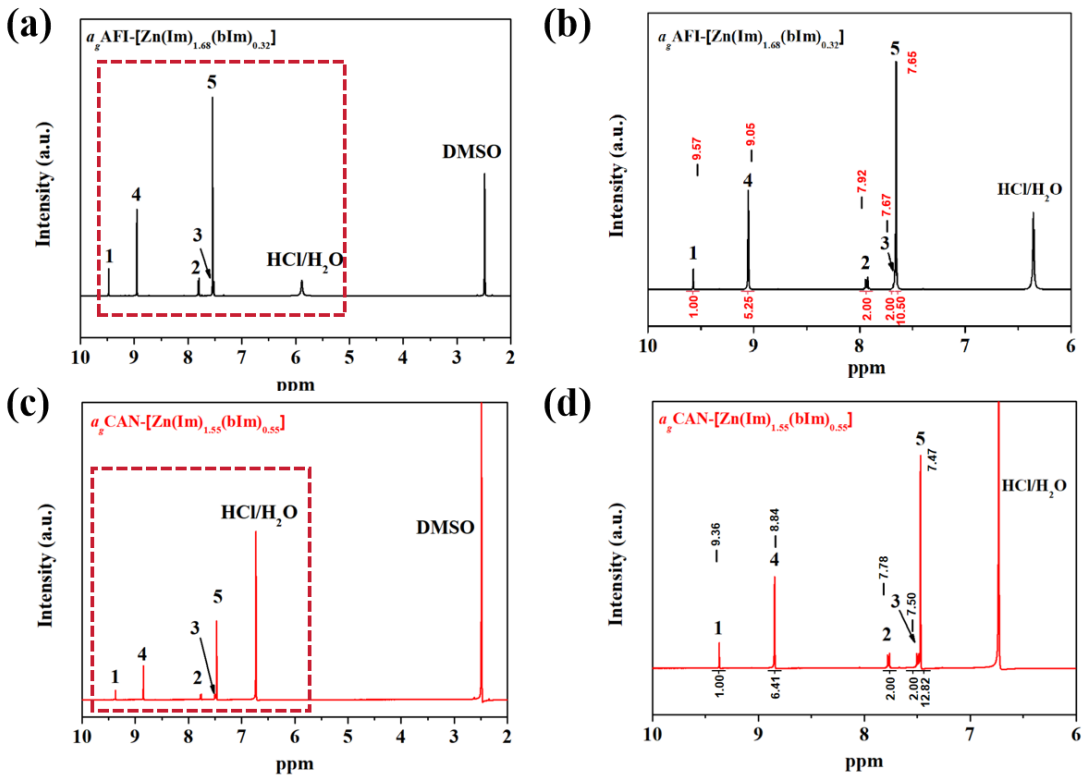

Fig. S10 ^{1}H NMR and Enlarged aromatic region for (a, b) a_gAFI-[Zn(Im)$_{1.68}$(bIm)$_{0.32}$]

and (c, d) a_gCAN-[Zn(Im)$_{1.55}$(bIm)$_{0.45}$].

Reviewer #2 (Remarks to the Author):

The authors prepared two meltable MOFs, AFI-[Zn(Im)$_{1.68}$(bIm)$_{0.32}$] and CAN-[Zn(Im)$_{1.73}$(bIm)$_{0.27}$], with large 12-membered rings pores using both structure-directing agents and mixed organic ligands. The enhanced porosity carries over to the glass upon melt quenching, resulting in high H_2, CO_2 and CH_4 adsorption capacities. Further, a free-standing a_gAFI-[Zn(Im)$_{1.68}$(bIm)$_{0.32}$] membrane was fabricated, showing very high gas permeance of around 104 GPU for CO_2 and CO_2/N_2 selectivity of around 15. The research is valuable. However, some critical points need to be elaborated to provide a clearer understanding. The paper could be published after addressing the concerns raised below:

Comment 1. *The BET surface areas of AFI-[Zn(Im)$_{1.68}$(bIm)$_{0.32}$] (1015 m^2/g) are basically same with that of AFI-[Zn(Im)$_2$] (1103 m^2/g). The result is different from normal cognition. Often, the N_2 adsorption amounts would decrease with the increase content of bulky bIm ligand. Besides, whether the bIm content in the AFI-[Zn(Im)$_{2-x}$(bIm)$_x$] sample could be adjusted?*

Response. We thank the reviewer for this comment.

The following content has been added in the revised manuscript (lines 148-152, page 6).

The N_2 adsorption amounts decrease after adding bulky bIm ligand in the framework, for example, the BET decreased from 1155 m^2/g to 1073 m^2/g for AFI-[Zn(Im)$_2$] and AFI-[Zn(Im)$_{1.68}$(bIm)$_{0.32}$], from 1033 m^2/g to 603 m^2/g for CAN-[Zn(Im)$_2$] and CAN-[Zn(Im)$_{1.73}$(bIm)$_{0.27}$].

The effects of bIm content on the performance of ZIF-62[27] and ZIF-8[32] have been reported. Henke et.al[27] found that the bIm linker partially occupies two of the four available imidazole salt positions in the ZIF-62 structure. By reducing the ratio of Im and bIm, the T_m of ZIF-62 can be reduced from 703 K to 643 K. The pore size distribution indicates that during the melting and formation of a_gZIF-62, small cavities (with a diameter of approximately 3.5 Å) completely disappear, but medium-sized cavities (with a diameter of 5-6 Å) are significantly preserved, and even new larger cavities (with a diameter of 8 Å) are formed. In previous studies[32, 33], bIm was used to

replace one of the three mIm joints in ZIF-8. As the content of bIm increased, the pore size significantly decreased, the pore size distribution narrowed, and the thermal stability also decreased.

These works indicate that the content of bIm effectively affects the properties of MOF and MOF glass, and related research will be conducted in the future.

27. Frentzel-Beyme L, Kloss M, Kolodzeiski P, Pallach R, Henke S. Meltable Mixed-Linker Zeolitic Imidazolate Frameworks and Their Microporous Glasses: From Melting Point Engineering to Selective Hydrocarbon Sorption. *J Am Chem Soc* **141**, 12362-12371 (2019).
32. Krokidas P, et al. On the efficient separation of gas mixtures with the mixed-linker zeolitic-imidazolate framework-7-8. *ACS Appl. Mater. Interfaces* **10** 39631-39644 (2018).
33. Thompson JA, et al. Hybrid zeolitic imidazolate frameworks: controlling framework porosity and functionality by mixed-linker synthesis. *Chem*. *Mater*. **24**, 1930-1936 (2012).

Comment 2. *The solubility coefficient (S) and diffusion coefficient (D) of membranes were measured by using constant volume-variable pressure method with pure gas (time-lag method). How about the pressure of the feed gas since the solubility coefficients are pressure related. Besides, it didn't give the N_2 adsorption isotherm of a_gAFI-[Zn(Im)$_{1.68}$(bIm)$_{0.32}$] and a_gZIF-62 at the membrane test temperature. How did the authors obtain the N_2 solubility coefficients?*

Response.

The solubility coefficient (*S*) and diffusion coefficient (*D*) of membranes were measured at 0.5 bar and 25 °C via the constant volume-variable pressure method with pure gas (time-lag method) on the Labthink instrument, G2/110-A. The initial step involved the application of a vacuum treatment to both the feed side and the permeation side. Subsequently, the cavity on the permeation side was sealed, the feed gas side was filled with test gas at a specified pressure, and it was ensured that a pressure differential of 0.5 bar was established on both sides of the glass membrane. Subsequently, the gas will permeate from the feed side to the permeation side under the pressure gradient. The permeance, solubility coefficient, and diffusion coefficient of the membrane can be calculated by processing the pressure data from the permeable side using the software. The diffusion coefficient (*D*, cm^2/s) was calculated by time-lag method (1):

$$D = \frac{l^2}{6\theta} \quad (1)$$

where l was the membrane thickness and θ was the time lag (s) before the steady straight-line relationship was calculated by the downstream pressure versus time plot. The solubility coefficient *S* ($cm^3(STP)\cdot cm^{-3}\cdot cmHg^{-1}$) was given by equation (2):

$$S = \frac{P}{D} \quad (2)$$

Comment 3. *The membrane stability under high pressure is very important to the industrial application of membrane gas separation. How about the effect of the transmembrane pressure on the gas separation stability of the self-supported glass membranes?*

Response.

Firstly, the CO_2 gas adsorption capacity of the a_gAFI-[Zn(Im)$_{1.68}$(bIm)$_{0.32}$] material was investigated under 30 bar. As the pressure increased, a_gAFI-[Zn(Im)$_{1.68}$(bIm)$_{0.32}$] continued to demonstrate a high CO_2 adsorption capacity, indicating that the material maintained its microporous structure under high pressure and demonstrated good pressure stability. Secondly, the integrated a_gAFI-[Zn(Im)$_{1.68}$(bIm)$_{0.32}$] glass membrane exhibited a certain degree of brittleness. During the gas permeance testing, the elevated gas pressure exerted on the membrane surface may result in the formation of macroscopic defects, such as membrane cracking. Finally, the a_gAFI-[Zn(Im)$_{1.68}$(bIm)$_{0.32}$] membrane exhibited a high gas permeance at relatively low feeding pressure, which made it a promising candidate for efficient separation processes.

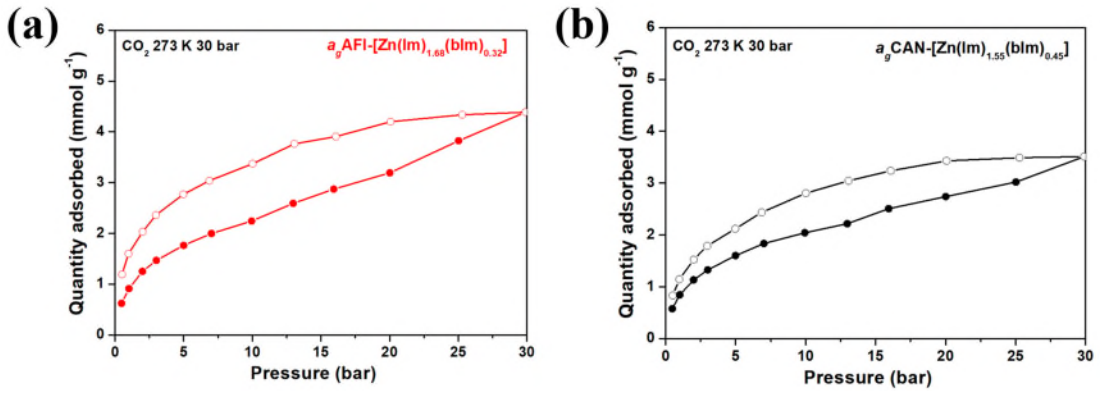

Fig. R3 the high-pressure CO_2 gas adsorption at 273 K and 30 bar (a) a_gAFI-[Zn(Im)$_{1.68}$(bIm)$_{0.32}$] and (b) a_gCAN-[Zn(Im)$_{1.55}$(bIm)$_{0.45}$].

Comment 4. *The supported a_gZIF-62 membrane showed CO_2/N_2 selectivity higher than 30 (Fig. 6c), why the self-supported thicker a_gZIF-62 membrane in this paper showed mixed selectivity lower than 10?*

Response.

According to the reported work, the a_gZIF-62/Al_2O_3 support had a CO_2 permeance of ~30 GPU for and a CO_2/N_2 selectivity of 35. As shown in Fig. R4, the cross-sectional

view of a_gZIF-62/Al_2O_3 support reveals that the overall a_gZIF-62 membrane is composed of three distinct parts: ZIF-62 of the surface layer, ZIF-62 of the infiltration layer, and ZIF-62 inside the porous Al_2O_3 support. According to the synthesis method of ZIF-62/Al_2O_3 support, the Al_2O_3 support disks (18 mm in diameter, 1000 μm in thickness) was firstly placed horizontally in a Teflon-lined stainless-steel autoclave which was filled with synthesis solution (exactly the same as preparing ZIF-62 powder), and then heated at 100 °C in an oven for 48 h. Afterwards, the support was dried at 100 °C overnight. From this, it can be inferred that ZIF-62 penetrated into a porous Al_2O_3 support with a thickness of 1000 μm during the synthesis process, resulting in an effective separation layer thickness far greater than 60 μm.

When the membrane thickness is 60 μm, the permeance of a_gZIF-62/AAO is 30 GPU. As the effective membrane thickness increases, the permeance of a_gZIF-62/AAO will further decrease, while the CO_2/N_2 selectivity will further increase. Therefore, the higher thickness (>60 μm) of a_gZIF-62 resulted in a CO_2/N_2 selectivity of 35 in a_gZIF-62/Al_2O_3 support. It is evident that a_gZIF-62 containing supports are prone to pore penetration and interfacial compatibility issues, which in turn presents an opportunity for further enhancement of the membrane's separation performance. In this work, the self-supported a_gZIF-62 membrane was prepared with a thickness of ~200 μm. The a_gZIF-62 membrane with independent support layer resulted in an improvement in permeance, although this was accompanied by a partial reduction in CO_2/N_2 selectivity. The explanation has been added into the revised manuscript (lines 407-411, page 16), marked in red. The support layer on a_gZIF-62/AAO surface can penetrate and increase the actual thickness of the composite membrane, thereby enhancing the CO_2/N_2 separation performance. Consequently, the CO_2/N_2 selectivity of the a_gZIF-62/AAO membrane as in the literature is higher than that of the self-supported a_gZIF-62 in this work.

Comment 5. *In line 281, the authors considered that the separation mechanism of a_gAFI-[Zn(Im)$_{1.68}$(bIm)$_{0.32}$] membrane was through molecular sieving. However, as can be seen from Table S4, the CH_4/N_2 diffusion selectivity was around 1 and the membrane performance was mainly attributed to the adsorption selectivity. The HR-TEM dark field images of a_gAFI-[Zn(Im)$_{1.68}$(bIm)$_{0.32}$] membrane also indicated that the transport channel is at the nanoscale (Fig. S14), which is difficult to achieve efficient molecular sieve separation.*

Response.

The question you posed regarding the separation mechanism of a_gAFI-[$Zn(Im)_{1.68}(bIm)_{0.32}$] membrane is a valuable contribution to this work. As you have stated, the CH_4/N_2 diffusion selectivity from the Table S8 is approximately 1, indicating that diffusion selectivity has a limited contribution to separation performance. The primary driving force behind the separation performance of CH_4/N_2 by the a_gAFI-[$Zn(Im)_{1.68}(bIm)_{0.32}$] membrane is adsorption-driven selectivity, rather than the molecular sieving.

The nonpolar molecules CH_4 and N_2 exhibit similar boiling points and kinetic diameters (CH_4: 3.80 Å, N_2: 3.64 Å), rendering them a prototypical system exhibiting difficulty in achieving effective separation. The disparity in the polarizabilities of N_2 and CH_4 (CH_4: 26.0×10^{-25} cm^3 cm^3, N_2: $17.6 \times 10\times10^{-25}$ cm^3) presents a potential avenue for enhancing the separation process by differentiating their interactions with the MOF materials. Furthermore, the adsorption curves of CH_4 and N_2 demonstrate that a_gAFI-[$Zn(Im)_{1.68}(bIm)_{0.32}$] exhibits a higher adsorption capacity for CH_4 than for N_2. Hence, the gas separation performance of the a_gAFI-[$Zn(Im)_{1.68}(bIm)_{0.32}$] membrane for CH_4/N_2 was primarily determined by adsorption selectivity, as evidenced by the results of gas adsorption and permeation testing.

The dark field images of HR-TEM demonstrate that the transport channel size in the membrane is at the nanoscale level, which typically necessitates more precise pore size control for molecular sieve mechanisms. Accordingly, we accept your proposal and will indicate in the revised manuscript that the performance of the a_gAFI-[$Zn(Im)_{1.68}(bIm)_{0.32}$] membrane for CH_4/N_2 is primarily determined by adsorption selectivity, as evidenced by the results of gas adsorption and permeation testing.

This explanation has already been revised to pages 13-14, lines 336-340 of the revised manuscript, marked in red.

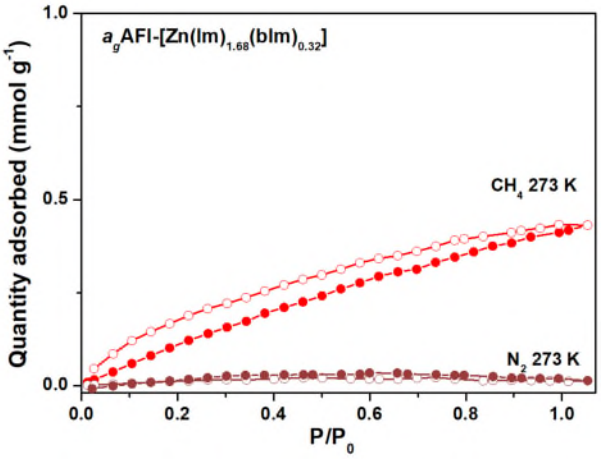

Fig. S24 The CH_4 and N_2 adsorption-desorption curves at 273 K for a_gAFI-[Zn(Im)$_{1.68}$(bIm)$_{0.32}$].

Reviewer #3 (Remarks to the Author):

In this work, the authors reported the preparation of MOF glass membranes with large pore sizes for high-permanence gas separation. The results would be important for MOF and membrane materials in this hot field. However, several important issues should be addressed before Nature Communications considers accepting it.

Comment 1. *Have the SDAs been removed before the glass conversion process? If not, what is the effect of SDAs on the pore structure of converted MOF glass?*

Response. We would like to express our gratitude for your careful review and valuable comments on our work.

As shown in the TGA and ^{1}H NMR results, SDAs have been removed before the glass conversion process.

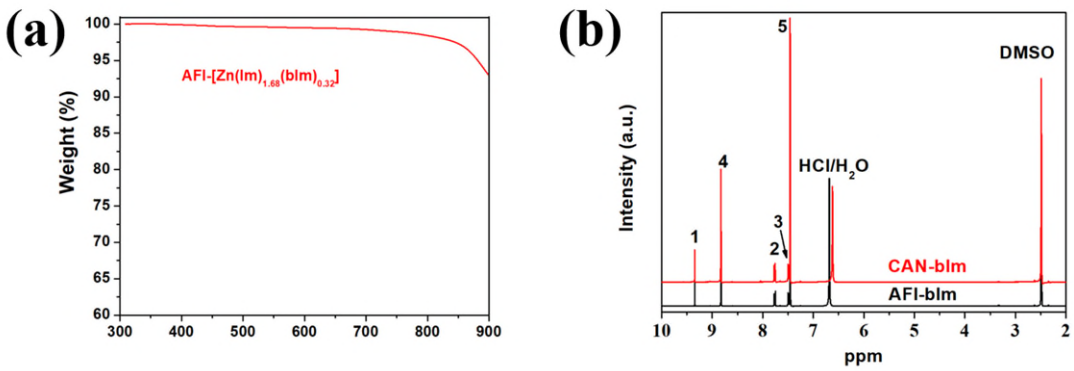

Fig. R5 TGA and ^{1}H NMR result of AFI-[Zn(Im)$_{1.68}$(bIm)$_{0.32}$].

Comment 2. Do the mixed ligands affect the melting point and MOF glass membrane preparation?

Response.

This is indeed an urgent issue that needs to be considered at present, and relevant work is already underway. Further research will be conducted in the next article.

The effects of bIm content on the performance of ZIF-62[27] and ZIF-8[32] have been reported. Henke et.al[27] found that the bIm linker partially occupies two of the four available imidazole salt positions in the ZIF-62 structure. By reducing the ratio of Im and bIm, the T_m of ZIF-62 can be reduced from 703 K to 643 K. The pore size distribution indicates that during the melting and formation of a_gZIF-62, small cavities (with a diameter of approximately 3.5 Å) completely disappear, but medium-sized cavities (with a diameter of 5-6 Å) are significantly preserved, and even new larger cavities (with a diameter of 8 Å) are formed. In previous studies[32, 33], bIm was used to replace one of the three mIm joints in ZIF-8. As the content of bIm increased, the pore size significantly decreased, the pore size distribution narrowed, and the thermal stability also decreased.

These works indicate that the content of bIm effectively affects the properties of MOF and MOF glass, and related research will be conducted in the future.

27. Frentzel-Beyme L, Kloss M, Kolodzeiski P, Pallach R, Henke S. Meltable Mixed-Linker Zeolitic Imidazolate Frameworks and Their Microporous Glasses: From Melting Point Engineering to Selective Hydrocarbon Sorption. *J Am Chem Soc* **141**, 12362-12371 (2019).
32. Krokidas P, et al. On the efficient separation of gas mixtures with the mixed-linker zeolitic-imidazolate framework-7-8. *ACS Appl. Mater. Interfaces* **10** 39631-39644 (2018).
33. Thompson JA, et al. Hybrid zeolitic imidazolate frameworks: controlling framework porosity and functionality by mixed-linker synthesis. *Chem*. *Mater*. **24**, 1930-1936 (2012).

Comment 3. *The mechanical stability test should be carried out on the membrane samples.*

Response.

As shown in Fig. S17, the mechanical properties of the ZIFs glass, a_gAFI-[$Zn(Im)_{1.68}(bIm)_{0.32}$] and a_gCAN-[$Zn(Im)_{1.55}(bIm)_{0.45}$], have been evaluated by nanoindentation testing, which indicates the mechanical strength of the molten glass. Furthermore, high-pressure CO_2 adsorption tests were conducted on a_gAFI-[$Zn(Im)_{1.68}(bIm)_{0.32}$] and a_gCAN-[$Zn(Im)_{1.55}(bIm)_{0.45}$]. The findings indicate that the two materials are capable of maintaining their microporous structure under a test pressure of 30 bar. In addition, the stability of continuous long-term penetration testing for 120 hours also demonstrated that a_gAFI-[$Zn(Im)_{1.68}(bIm)_{0.32}$] has good separation

stability.

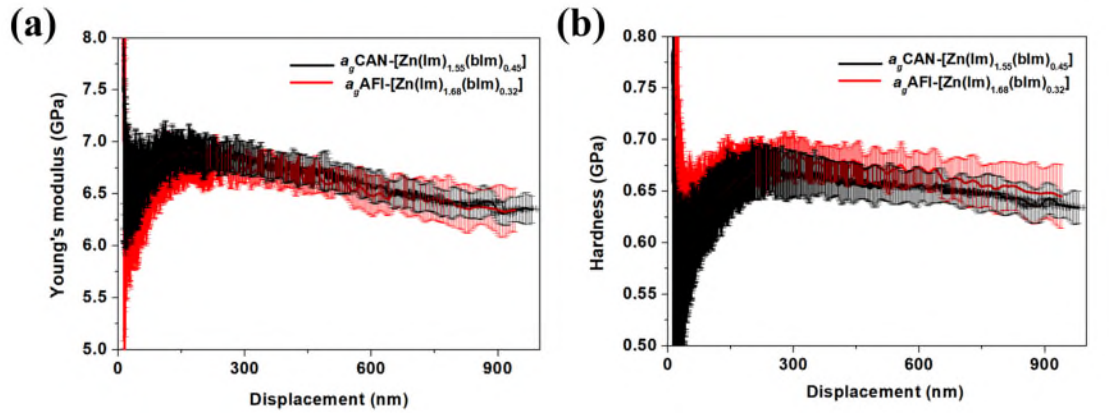

Fig. S17 Nano-indentation results of (a) a_gAFI-[Zn(Im)$_{1.68}$(bIm)$_{0.32}$] and (b) a_gCAN-[Zn(Im)$_{1.55}$(bIm)$_{0.45}$].

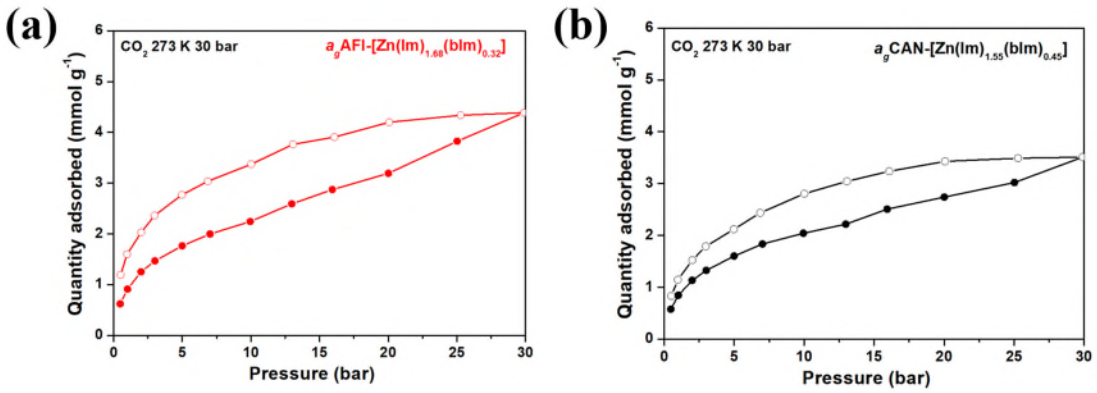

Fig. R3 High pressure CO_2 adsorption-desorption curve at 30 bar and 273 K of (a) a_gAFI-[Zn(Im)$_{1.68}$(bIm)$_{0.32}$] and (b) a_gCAN- [Zn(Im)$_{1.55}$(bIm)$_{0.45}$].

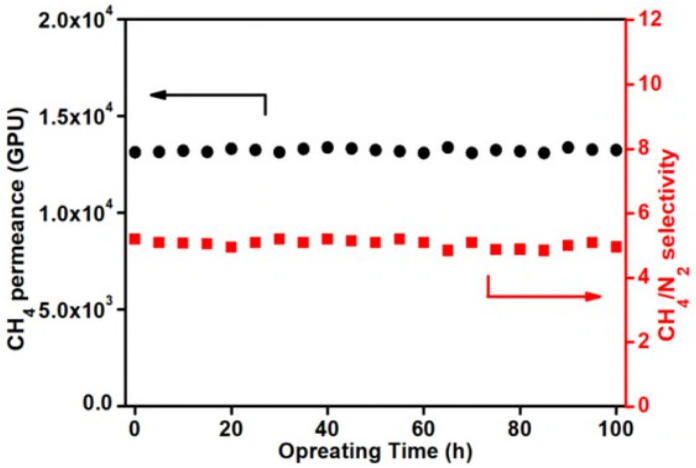

Fig. S25. Long-term mixed-gas separation performance of the a_gAFI-[Zn(Im)$_{1.68}$(bIm)$_{0.32}$] membrane (200 μm).

Comment 4. *The pore size distribution of this work's MOF and MOF glass materials*

should be summarized in the main text.

Response.

The pore volumes and pore size distributions of a_gAFI-[Zn(Im)$_{1.68}$(bIm)$_{0.32}$] and a_gCAN-[Zn(Im)$_{1.55}$(bIm)$_{0.45}$]were tested by CO_2 adsorption-desorption curves at 195 K, and the comparison was made with other glasses.

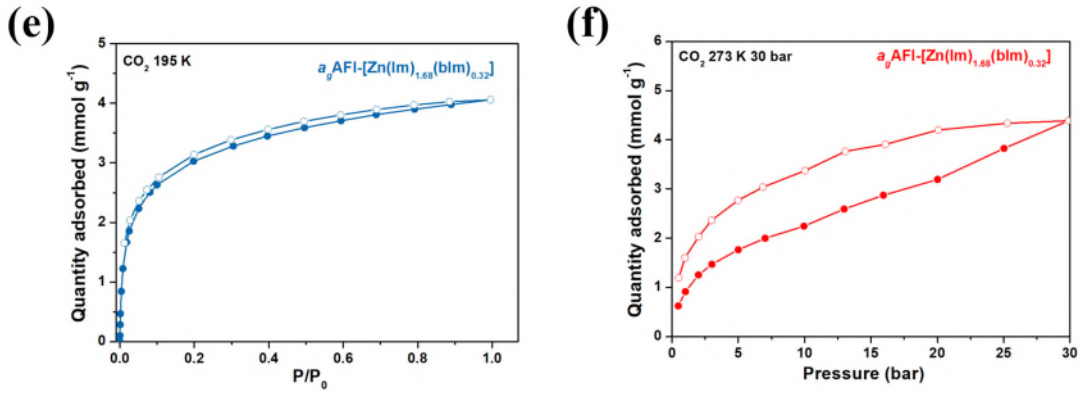

Fig. 4 Gas isotherms of a_gAFI-[Zn(Im)$_{1.68}$(bIm)$_{0.32}$] tested by (e) CO_2 at 195 K and (f) CO_2 at 273 K and 30 bar.

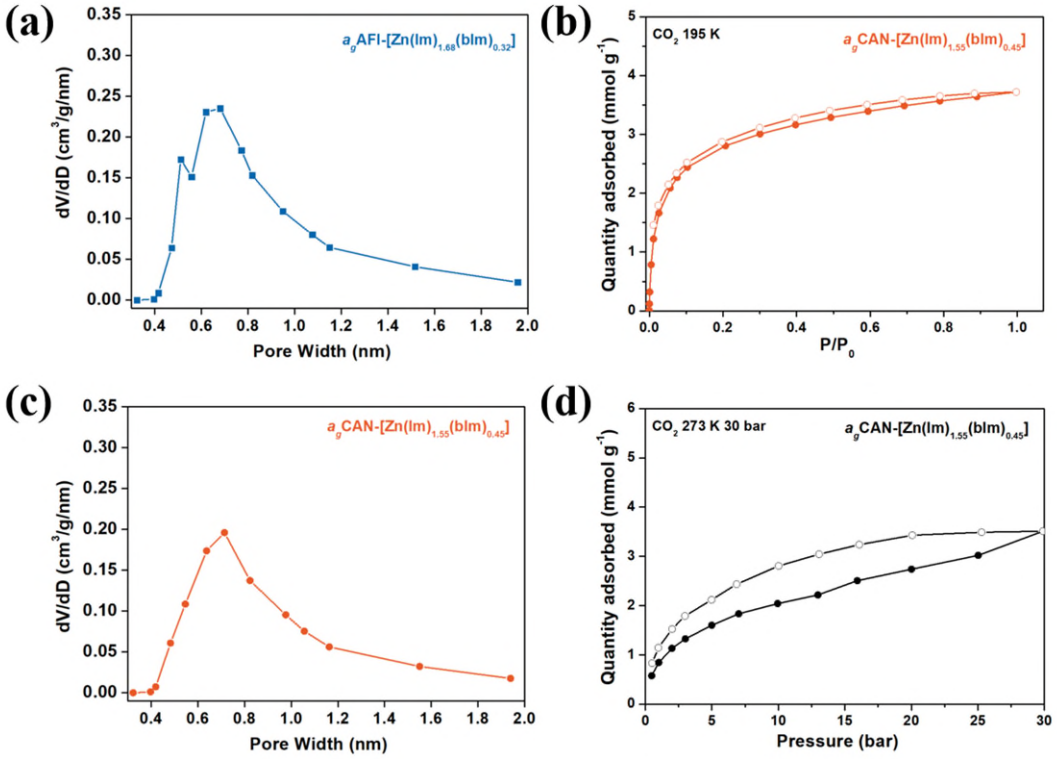

Fig. S19 (a) Pore size distribution of a_gAFI-[Zn(Im)$_{1.68}$(bIm)$_{0.32}$] obtained by CO_2 isotherms at 195 K. (b) CO_2 isotherms at 195 K, (c) pore size distribution, and (d) the high-pressure CO_2 adsorption at 273 K and 30 bar for a_gCAN-Zn(Im)$_{1.55}$(bIm)$_{0.45}$].

Tabel 1 Gas capacities, BET values, and pore volumes obtained by 195 K CO_2 isotherms.

Sample	Method	V_{ads} (cm^3/g)	n_{ads} (mmol/g)	S_{BET} (m^2/g)	V_{pore} (cm^3/g)	Ref.
a_gZIF-62	195 K CO_2	74.8	3.34	200	0.12	34
a_gTIF-4	195 K CO_2	76.2	3.4	204	0.12	34
a_gZIF-4	195 K CO_2	63.6	2.84	187	0.10	34
a_gZIF-67-$mim_{0.18}im_{0.68}bim_{0.14}$	195 K CO_2	118.5	5.3	316	0.18	35
a_gZIF-8-$mim_{0.15}im_{0.74}bim_{0.11}$	195 K CO_2	125.0	5.6	403	0.20	35
a_gCAN-bIm-$[Zn(Im)_{1.55}(bIm)_{0.45}]$	195 K CO_2	83.5	3.72	241	0.14	This work
a_gAFI-$[Zn(Im)_{1.68}(bIm)_{0.32}]$	195 K CO_2	91.0	4.06	285	0.16	This work

Comment 5. *Why do AFI-$[Zn(Im)_{1.68}(bIm)_{0.32}]$ and CAN-$[Zn(Im)_{1.73}(bIm)_{0.27}]$, both of which possess high porosity, exhibit significantly different pore structure after glass conversion? More discussion is needed.*

Response.

In the previous version of the manuscript, the synthesized CAN-$[Zn(Im)_{1.73}(bIm)_{0.27}]$ sample shows many disordered crystal structures, resulting in low XRD intensity and low N_2 adsorption amount.

In the amended manuscript, the synthesis of CAN-$[Zn(Im)_{1.73}(bIm)_{0.27}]$ has been optimized, which results in higher gas adsorption amount of both crystal and glass.

This explanation has already been revised to page 6, lines 169-175 of the revised manuscript, marked in red.

The N_2 adsorption amounts decrease after adding bulky bIm ligand in the framework, for example, the BET decreased from 1155 m^2/g to 1073 m^2/g for AFI-$[Zn(Im)_2]$ and a_gAFI-$[Zn(Im)_{1.68}(bIm)_{0.32}]$, from 1033 m^2/g to 603 m^2/g for CAN-$[Zn(Im)_2]$ and a_gCAN-$[Zn(Im)_{1.55}(bIm)_{0.45}]$. The lower BET surface area of CAN-$[Zn(Im)_{1.73}(bIm)_{0.27}]$ than CAN-$[Zn(Im)_2]$ (Supplementary Fig. 3) is attributed to that the synthesized CAN-$[Zn(Im)_{1.73}(bIm)_{0.27}]$ has low crystallinity, resulting in low porosity of the crystals.

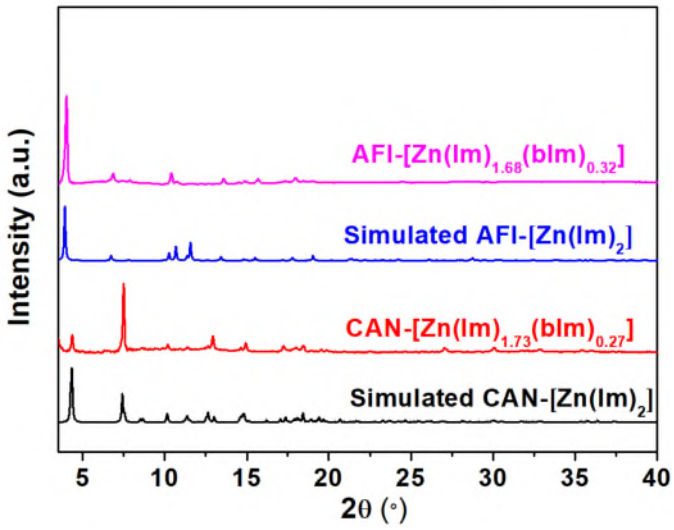

Fig. 2 XRD patterns of AFI-[$Zn(Im)_{1.68}(bIm)_{0.32}$] and CAN-[$Zn(Im)_{1.73}(bIm)_{0.27}$].

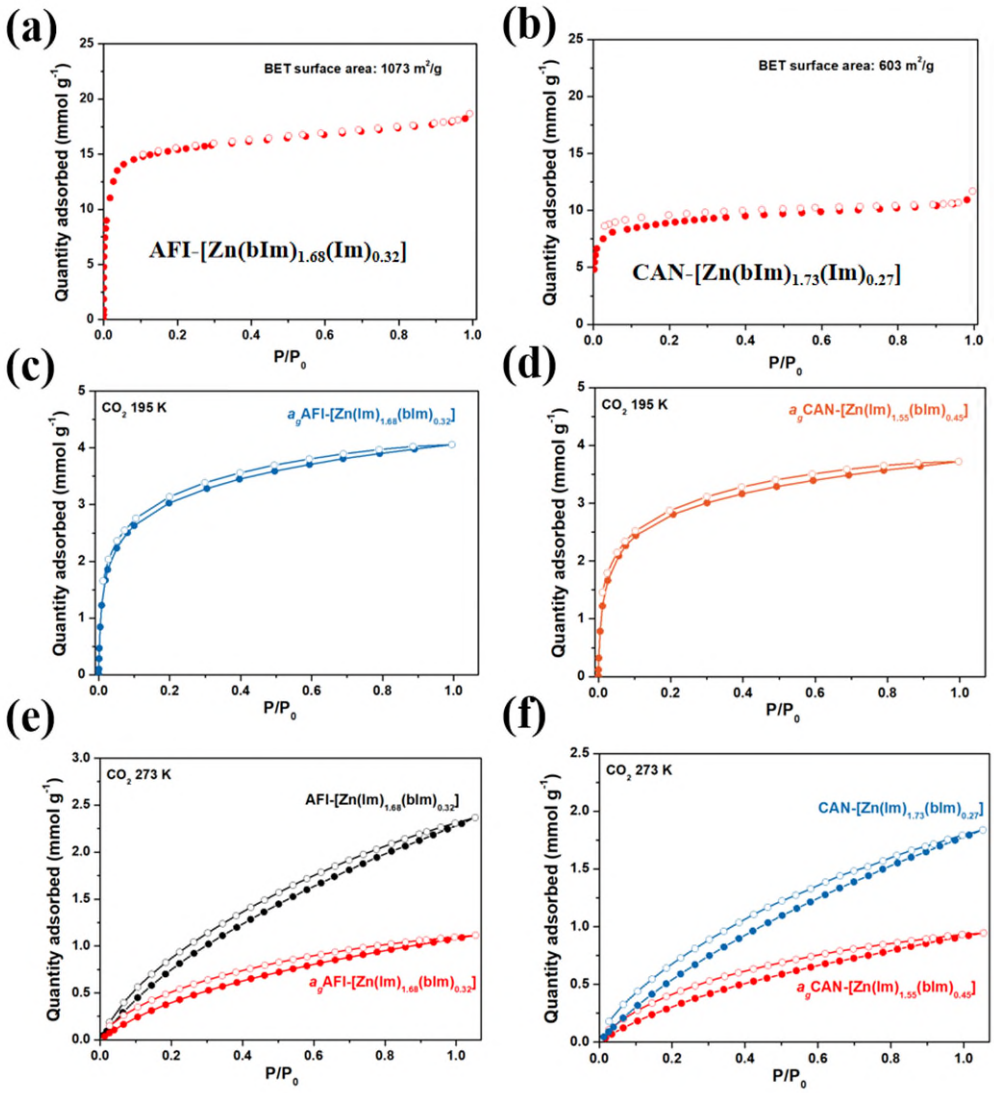

Fig. R6 Gas adsorption desorption curves for (a-b) 77 K N_2 (c-d) 195 K CO_2, and (e-f) 273 K CO_2.

Comment 6. *Page 6, line 141-3, the authors stated, "The powder XRD patterns of .... (Fig.1b)." Please check the corresponding figure number here.*

Response.

Page 6, line 140-142, the powder XRD patterns of AFI-[$Zn(Im)_{1.68}(bIm)_{0.32}$] and CAN-[$Zn(Im)_{1.73}(bIm)_{0.27}$] were similar to the simulated patterns of AFI-[$Zn(Im)_2$] and CAN-[$Zn(Im)_2$] (Fig. 2b).

Comment 7. *Please enlarge the font size in Fig 2e and 2f and pinpoint every TA, Tm, and T_g with arrows. Furthermore, on Page 10, line 242- 5, the authors noted, "Moreover, the large solvent molecules used as SDAs in the synthesis ....that possibly decrease the decomposition temperature or increase the melting point of the resultant MOF crystals." However, the Tm of the two materials reported in this work does not increase compared to ZIF-62. Since this study involves a variety of temperature values for different materials, it is recommended that the results be summarized in a table more clearly.*

Response.

The temperature values (T_A, T_m, *and* T_g) of various materials in this work were indicated by arrows in Figure 2 and summarized in Table 1.

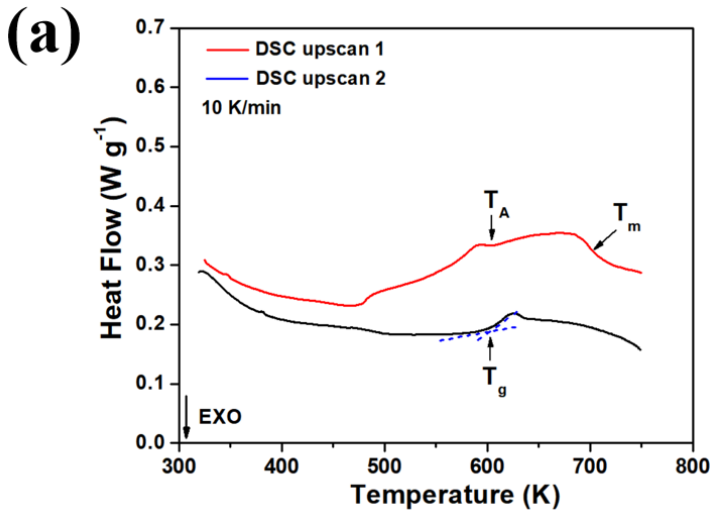

Fig. S12 DSC curves of AFI-[$Zn(Im)_{1.68}(bIm)_{0.32}$] at varying heating rates (a) 10 K.

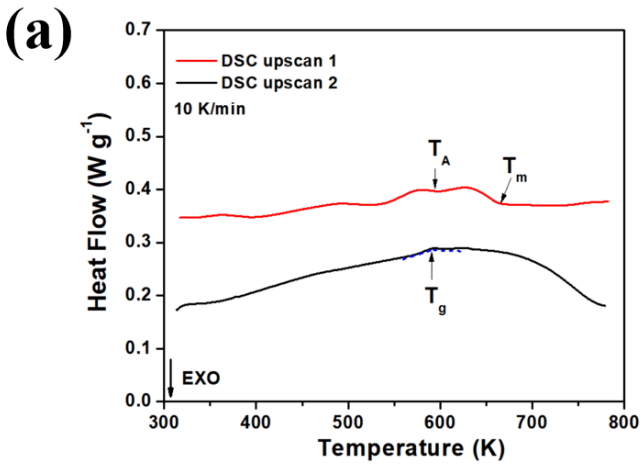

Fig. S13 DSC curves of CAN-$[Zn(Im)_{1.73}(bIm)_{0.27}]$ at varying heating rates (a) 10 K.

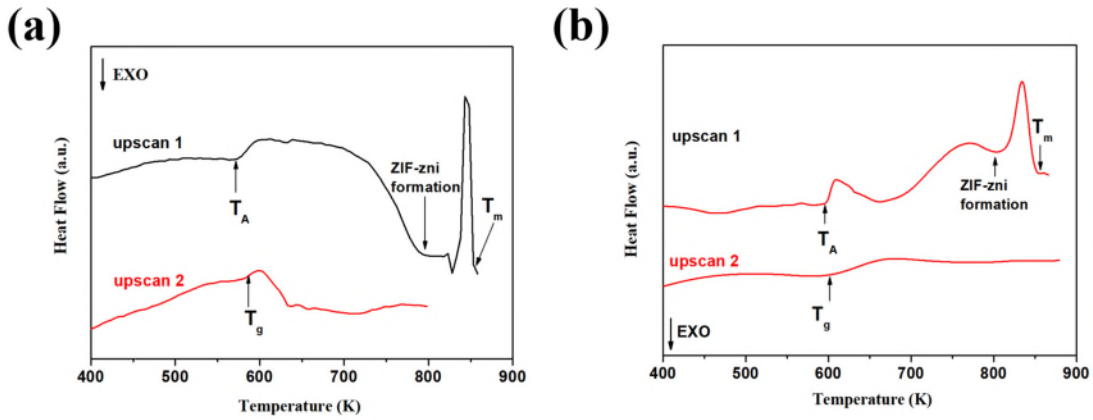

Fig. S5 (a) DSC curves of AFI-$[Zn(Im)_2]$ and CAN-$[Zn(Im)_2]$ with heating rate of 10 K/min under Ar.

Table S3. Summary of the temperature values of AFI-$[Zn(Im)_{1.68}(bIm)_{0.32}]$ obtained from the DSC data.

Material	Composition	T_m (K)	T_g (K)	T_A (K)
AFI-$[Zn(Im)_{1.68}(bIm)_{0.32}]$	$Zn(Im)_{1.68}(bIm)_{0.32}$	705	607	618
CAN-$[Zn(Im)_{1.73}(bIm)_{0.27}]$	$Zn(Im)_{1.7.}(bIm)_{0.27}$	670	591	595
AFI-$[Zn(Im)_2]$	$Zn(Im)_2$	853	588	573
CAN-$[Zn(Im)_2]$	$Zn(Im)_2$	853	600	598

Comment 8. *Some units for the X-axis in Fig. 4 are wrong. Relative pressure units (e.g.,*

P/P₀) should be used instead of absolute pressure units when testing under critical conditions.

Response.

The relevant relative pressure unit (*P/P₀*) has been corrected in Fig. 4, and we have also amended similar errors in other figures.

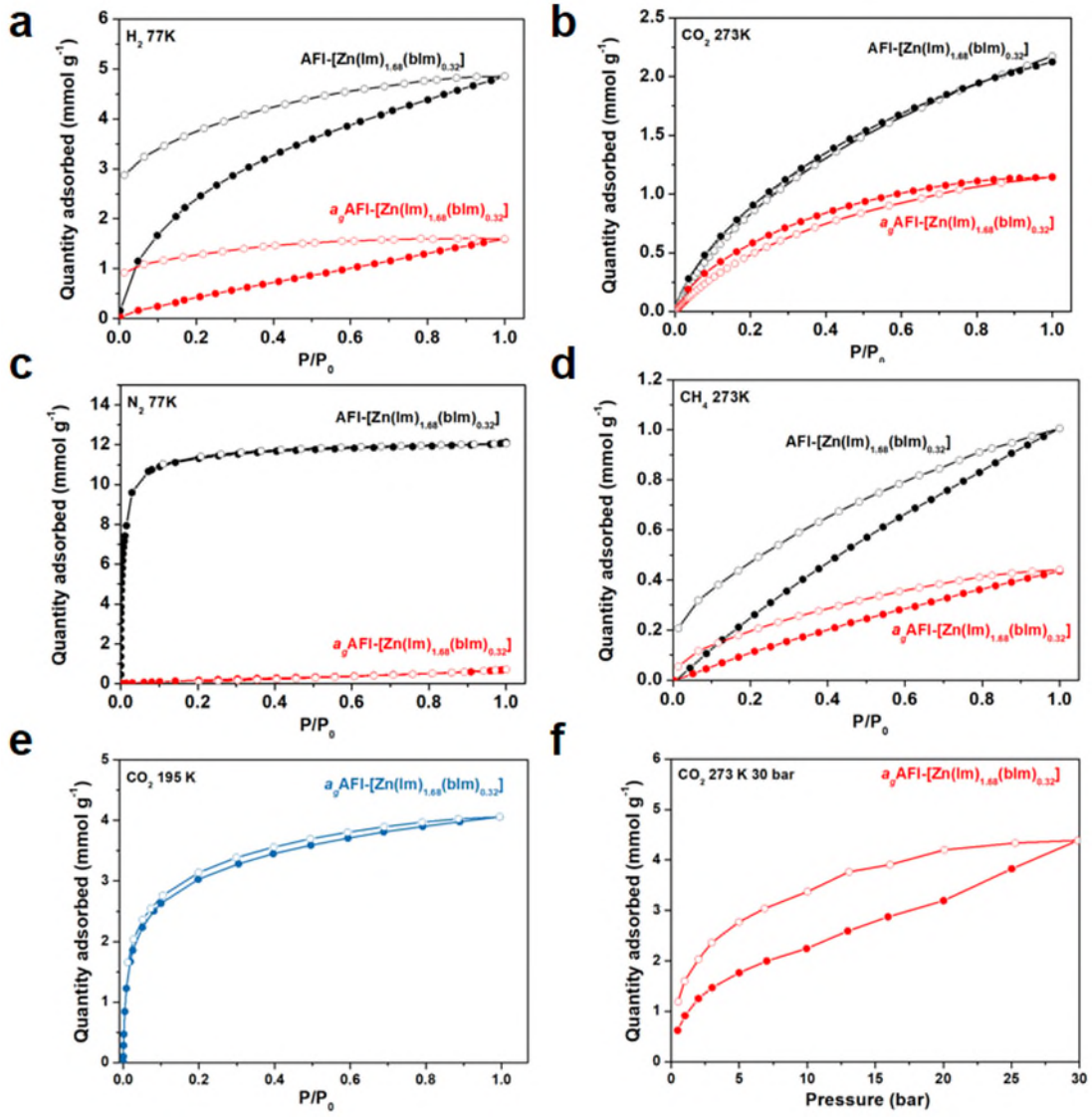

Fig. 4 Gas isotherms of AFI-[$Zn(Im)_{1.68}(bIm)_{0.32}$] and a_gAFI-[$Zn(Im)_{1.68}(bIm)_{0.32}$] tested by (a) H_2 at 77 K, (b) CO_2 at 273 K, (c) N_2 at 77 K, (d) CH_4 at 273K, (e) CO_2 at 195 K, and (f) CO_2 at 273 K and 30 bar.

Comment 9. *Supplementing the SEM images of membrane surface morphology in Fig 5 is suggested.*

Response.

We have supplemented the SEM images of the membrane surface at different

magnifications (scale bar was 10 μm, 1 μm, 400 nm), which are shown in Fig. 5.

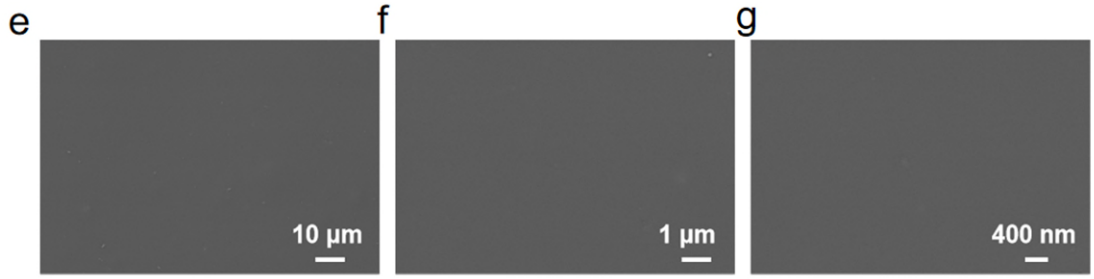

Fig. 5 The SEM images of the membrane surface (e) 10 μm, (f) 1 μm, and (g) 400 nm.

Comment 10. *Page 11, line 277, the authors noted that "The gas permeance decreased with increasing the kinetic diameter of gas molecules." However, the behavior of the three gases studied in this work generally does not follow this trend. Please expand on this to avoid any ambiguity.*

Response.

To obviate any potential ambiguity, the sentence (Page 11, line 277, "The gas permeance decreased with increasing the kinetic diameter of gas molecules.") has been deleted. Indeed, although the kinetic diameter of CH_4 is larger than that of N_2, the permeance of the a_gAFI-[$Zn(Im)_{1.68}(bIm)_{0.32}$] membrane for CH_4 is higher than that of N_2.

The nonpolar molecules CH_4 and N_2 exhibit similar boiling points and kinetic diameters (CH_4: 3.80 Å, N_2: 3.64 Å), rendering them a prototypical system exhibiting difficulty in achieving effective separation. The disparity in the polarizabilities of N_2 and CH_4 (CH_4: 26.0×10^{-25} cm^3 cm^3, N_2: $17.6 \times 10\times10^{-25}$ cm^3) presents a potential avenue for enhancing the separation process by differentiating their interactions with the MOF materials. Furthermore, as shown in Fig. S24, the adsorption curves of CH_4 and N_2 demonstrate that a_gAFI-[$Zn(Im)_{1.68}(bIm)_{0.32}$] exhibits a higher adsorption capacity for CH_4 than for N_2.

Accordingly, the permeance of the a_gAFI-[$Zn(Im)_{1.68}(bIm)_{0.32}$] membrane to CH_4 is higher than that of N_2, primarily due to its adsorption selectivity. The changes have been highlighted in red in the revised manuscript.

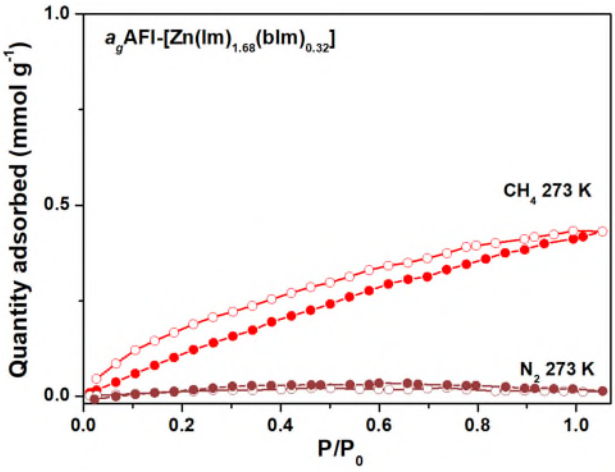

Fig. S24 The CH_4 and N_2 adsorption-desorption curves at 273 K for a_gAFI-[Zn(Im)$_{1.68}$(bIm)$_{0.32}$].

Comment 11. *The membrane thickness is several hundred micrometers, and the gas adsorption on the membrane materials is not very high, but the gas permeance is very high. More commentary and explanation should be provided on this point. Dead-end pores may be formed in the MOF glass membranes, reducing the effective membrane thickness.*

Response.

It is acknowledged that despite the thickness of the a_gAFI-[Zn(Im)$_{1.68}$(bIm)$_{0.32}$] membrane being approximately 200 μm, it exhibits an high CO_2 gas permeance. This can be attributed to two principal factors. The a_gAFI-[Zn(Im)$_{1.68}$(bIm)$_{0.32}$] membrane had the developed pore continuity and improved porosity (as evidenced by high-pressure CO_2 adsorption, pore volume, and TEM), which effectively reduced the path resistance of gas molecules through the membrane. The considerable enhancement in permeance suggested that the primary gas transport mechanism may be direct diffusion through the pores, with the separation mechanism being dominated by the synergistic interaction forces. Additionally, the He gas density test indicated the formation of a series of dead-end pores in the a_gAFI-[Zn(Im)$_{1.68}$(bIm)$_{0.32}$] membrane, which reduced the actual separation thickness of the glass membrane and enhanced the gas permeance. This explanation has already been revised to page 16, lines 407-415 of the revised manuscript, marked in red.

Reviewer #4 (Remarks to the Author):

This manuscript reports the strategy of enhancing the porosity of MOF glasses by topological engineering of meltable crystalline ZIFs, which is novel and effective. The enhancement of gas separation performance of the ZIF glass membrane is very impressive. However, some issues need to be further discussed. Thus, I would recommend minor revision before acceptance.

Comment 1. *Conduct additional experiments to validate the maximum bIm substitution ratios of AFI-[Zn(Im)$_{1-x}$(bIm)$_x$] and CAN-[Zn(Im)$_{1-x}$(bIm)$_x$] hybrids, including comprehensive characterization of their structural and pore properties.*

Response. We appreciate the reviewer's comment.

This is indeed an urgent issue that needs to be considered at present, and relevant work is already underway. Further research will be conducted in the next article.

The effects of bIm content on the performance of ZIF-62[27] and ZIF-8[32] have been reported. Henke et.al[27] found that the bIm linker partially occupies two of the four available imidazole salt positions in the ZIF-62 structure. By reducing the ratio of Im and bIm, the T_m of ZIF-62 can be reduced from 703 K to 643 K. The pore size distribution indicates that during the melting and formation of a_gZIF-62, small cavities (with a diameter of approximately 3.5 Å) completely disappear, but medium-sized cavities (with a diameter of 5-6 Å) are significantly preserved, and even new larger cavities (with a diameter of 8 Å) are formed. In previous studies[32, 33], bIm was used to replace one of the three mIm joints in ZIF-8. As the content of bIm increased, the pore size significantly decreased, the pore size distribution narrowed, and the thermal stability also decreased.

These works indicate that the content of bIm effectively affects the properties of MOF and MOF glass, and related research will be conducted in the future.

27. Frentzel-Beyme L, Kloss M, Kolodzeiski P, Pallach R, Henke S. Meltable Mixed-Linker Zeolitic Imidazolate Frameworks and Their Microporous Glasses: From Melting Point Engineering to Selective Hydrocarbon Sorption. *J Am Chem Soc* **141**, 12362-12371 (2019).
32. Krokidas P, et al. On the efficient separation of gas mixtures with the mixed-linker zeolitic-imidazolate framework-7-8. *ACS Appl. Mater. Interfaces* **10** 39631-39644 (2018).
33. Thompson JA, et al. Hybrid zeolitic imidazolate frameworks: controlling framework porosity and functionality by mixed-linker synthesis. *Chem*. *Mater*. **24**, 1930-1936 (2012).

Comment 2. *The authors stated that the lower BET surface area of CAN-*

[Zn(Im)$_{1.73}$(bIm)$_{0.27}$] than CAN-[Zn(Im)$_2$] was attributed to the degree of disorder. Conduct additional experiments to increase the BET value, the as-synthesized CAN-[Zn(Im)$_{1.73}$(bIm)$_{0.27}$] can be immersed in dry acetone.

Response. We would like to express our gratitude for your careful review and valuable comments on our work.

The synthesized CAN was replaced with dry acetone three times a day for a total of three days. Subsequently, a white powder was obtained through high-speed centrifugation, and the remaining acetone was further removed by degassing at 100 ℃ to yield the dry CAN-[Zn(Im)$_{1.73}$(bIm)$_{0.27}$] and CAN-[Zn(Im)$_2$]. The BET results obtained for 77K N_2 isothermal indicated that CAN-[Zn(Im)$_2$] and CAN-[Zn(Im)$_{1.73}$(bIm)$_{0.27}$] were 1033 m²/g and 603 m²/g, respectively.

This explanation has already been revised to page 17, lines 446-448 of the revised manuscript, marked in red.

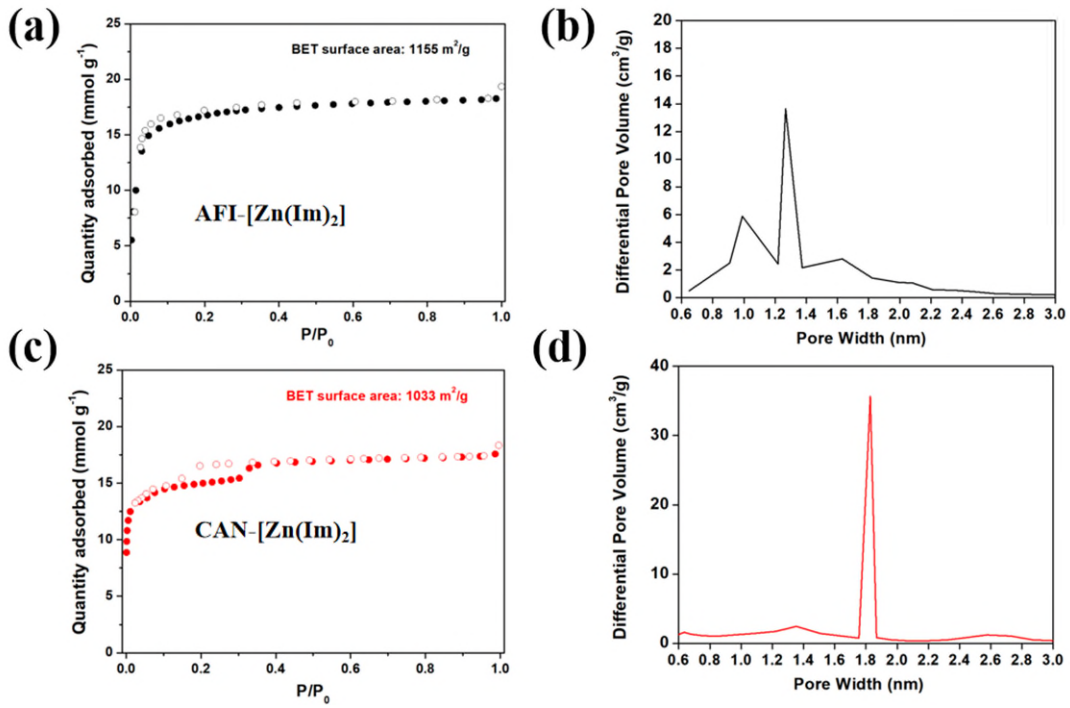

Fig. S3 N_2 isotherms of (a) AFI-[Zn(Im)$_2$] and (c) CAN-[Zn(Im)$_2$]; pore distribution of (b) AFI-[Zn(Im)$_2$] and (d) CAN-[Zn(Im)$_2$].

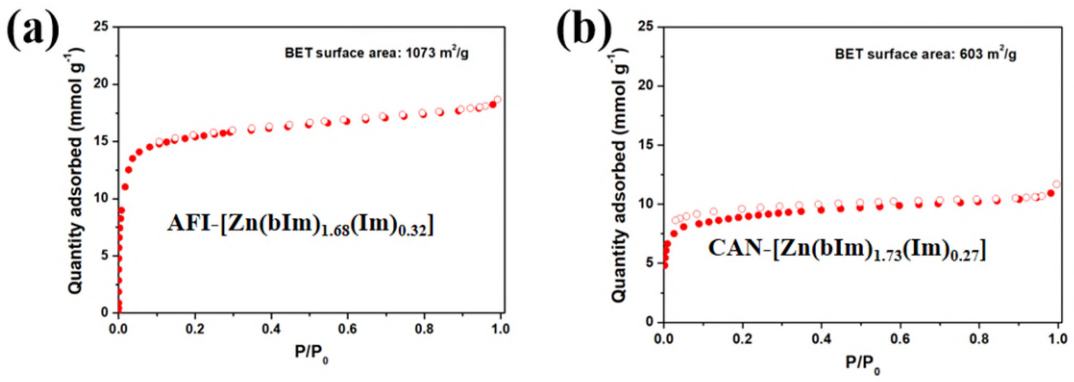

Fig. S7 N_2 isotherms of (a) AFI-[$Zn(Im)_{1.68}(bIm)_{0.32}$] and (b) CAN-[$Zn(Im)_{1.73}(bIm)_{0.27}$].

Comment 3. *Could the authors compare the porosity of AFI MOF before and after melt-quenching? Please also discuss the collapse process of pores in AFI MOF during melt-quenching. This is the key to validate the idea of this work.*

Response. We would like to express our gratitude for your careful review and valuable comments on our work.

Comparison shows that after vitrification, the adsorption capacity of a_gAFI-[$Zn(Im)_{1.68}(bIm)_{0.32}$] for various gases decreases, which is believed to be due to the partial collapse of the open pores in the crystalline MOFs during the melt quenching process, leading to a decrease in porosity. According to existing reports[1-3], it is speculated that the melting process of AFI-[$Zn(Im)_{1.68}(bIm)_{0.32}$] is first caused by the loss of the ordered structure of the crystal due to the increase in temperature, but the pore channels still exist, which is consistent with the PDF structure; When the temperature reaches the hot amorphous point, the remaining SDA undergoes desolvation and the first pore collapse occurs; When the temperature continues to rise and reaches the melting temperature, a porous "MOF liquid" is formed, but the liquid phase still retains the chemical configuration and coordination bonding mode of the solid phase; The final tempering resulted in stronger collapse of the pore portion, and the surface tension of the melt caused smooth edges, leading to shrinkage and increased density, forming a_gAFI-[$Zn(Im)_{1.68}(bIm)_{0.32}$].

1. R. Gaillac, P. Pullumbi, K.A. Beyer, K.W. Chapman, D.A. Keen, T.D. Bennett, F.-X. Coudert, Liquid metal–organic frameworks, Nature Materials 16 (2017) 1149.

2. Khudozhitkov A E, Ogiwara N, Donoshita M, et al. Dynamics of Linkers in Metal–Organic Framework Glasses [J]. Journal of the American Chemical Society, 2024, 146(19): 12950-12957.
3. Smirnova O, Hwang S, Sajzew R, et al. Precise control over gas-transporting channels in zeolitic imidazolate framework glasses [J]. Nature Materials, 2024, 23(2): 262-270.

Comment 4. *The thickness of the membrane is about 200 μm. Could the authors discuss the prospect of practical applications of that thick membrane?*

Response.

The explanation has been added to the revised manuscript (lines 390-399, pages 15-16) and highlighted in red.

The a_gAFI-[Zn(Im)$_{1.68}$(bIm)$_{0.32}$] membrane is suitable for assembling into disc type membrane modules. Although the packing density of disc type membrane modules is typically lower than that of spiral and hollow fibre modules, they can effectively inhibit concentration polarization of permeation gas, which is conducive to high-permeance membrane assembly. Disc type membrane modules can be designed to effectively handle gases in confined spaces, such as small pollution sources or compact waste gas treatment devices.

Comment 5. *The authors stated that the separation mechanism is molecular sieving. The kinetic diameter of CH_4 is larger than N_2. However, the membrane displays higher CH_4 permeance than N_2. Why?*

Response.

Indeed, the permeance of the a_gAFI-[Zn(Im)$_{1.68}$(bIm)$_{0.32}$] membrane to CH_4 is higher than that of N_2. The primary driving force behind the separation performance of CH_4/N_2 by the a_gAFI-[Zn(Im)$_{1.68}$(bIm)$_{0.32}$] membrane is adsorption-driven selectivity, rather than the molecular sieving.

The nonpolar molecules CH_4 and N_2 exhibit similar boiling points and kinetic diameters (CH_4: 3.80 Å, N_2: 3.64 Å), rendering them a prototypical system exhibiting difficulty in achieving effective separation. The disparity in the polarizabilities of N_2 and CH_4 (CH_4: 26.0×10^{-25} cm^3 cm³, N_2: $17.6 \times 10\times10^{-25}$ cm^3) presents a potential avenue for enhancing the separation process by differentiating their interactions with the MOF

materials. Furthermore, as shown in Fig. S11, the adsorption curves of CH_4 and N_2 demonstrate that a_gAFI-[$Zn(Im)_{1.68}(bIm)_{0.32}$] exhibits a higher adsorption capacity for CH_4 than for N_2.

Accordingly, we accept your proposal and will indicate in the revised manuscript that the performance of the a_gAFI-[$Zn(Im)_{1.68}(bIm)_{0.32}$] membrane for CH_4/N_2 is primarily determined by adsorption selectivity, as evidenced by the results of gas adsorption and permeation testing.

This explanation has already been added to revised manuscript (lines 336-340, pages 13-14), marked in red.

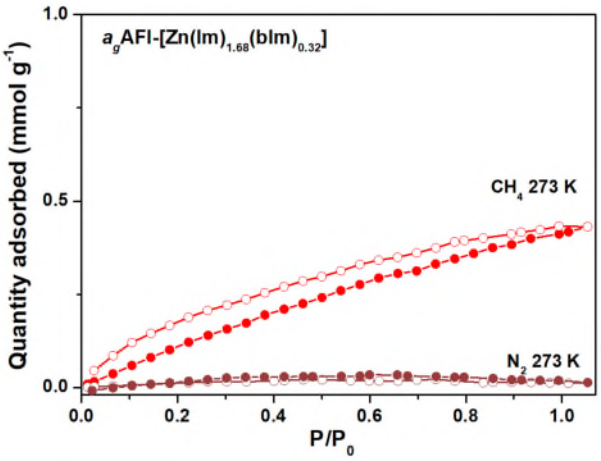

Fig. S24 The CH_4 and N_2 adsorption-desorption curves at 273 K for a_gAFI-[$Zn(Im)_{1.68}(bIm)_{0.32}$].

Comment 6. Please explain the extremely higher gas diffusivity of the a_gAFI than a_gZIF-62.

Response.

The a_gAFI-[$Zn(Im)_{1.68}(bIm)_{0.32}$] membrane had the developed pore continuity and improved porosity (as evidenced by high-pressure CO_2 adsorption, pore volume, and TEM), which effectively reduced the path resistance of gas molecules through the membrane. The considerable enhancement in permeance suggested that the primary gas transport mechanism may be direct diffusion through the pores, with the separation mechanism being dominated by the synergistic interaction forces. Therefore, the gas

diffusivity of a_gAFI-[Zn(Im)$_{1.68}$(bIm)$_{0.32}$] membrane was higher than that of a_gZIF-62. This explanation has already been added to the revised manuscript (lines 346-352, page 14), marked in red.

Comment 7. The authors stated that the a_gAFI shows advantages in precise manipulation of porosity compared with a_gZIF-62 foam. Please explain more here

Response. Thank the reviewer for their in-depth questions and suggestions on our work. The main factor for the formation of foam is the pore forming agent. If the pore forming agent is used to precisely control the pore structure, the uniformity of solid phase blending needs to be fully mixed evenly, and the gas decomposition and diffusion can be controlled. The existing experimental technology has not yet reached the ideal level, so the pore structure is still unclear. The topological structure of AFI-[Zn(Im)$_{1.68}$(bIm)$_{0.32}$] crystal is accurate, and its influence on the glass pore structure is fundamentally and directly related.

RESPONSE TO REVIEWERS' COMMENTS

Reviewer #1 (Remarks to the Author):

The authors have done a very good job in revising their manuscript and addressing my questions. Several additional experiments have been conducted, and the new data and its discussion in the manuscript significantly enhance the overall quality of the work. In my opinion, this is a valuable contribution to the MOF glass field, and I support its publication in Nature Communications. However, before publication, the authors need to address the following methodological issues:

Comments 1. *The pressure axis of many H_2, CO_2, and CH_4 sorption isotherms in the manuscript and supplementary information is erroneously labelled with p/p_0. Here, p_0 represents the saturation pressure (condensation pressure) of the respective gas at the isothermal measurement temperature. I believe most of these isotherms were measured at absolute pressures ranging from approximately 0 to 1 bar, not relative pressures of $p/p_0 = 1$. For H_2 at 77 K and for CO_2 and CH_4 at 273 K, p_0 is substantially higher than 1 bar. Additionally, p_0 is undefined for CO_2 at 195 K since liquid CO_2 (as present in the pores of the ZIF) does not exist in the phase diagram at this temperature. Except for the N_2 sorption isotherm recorded at 77 K, the sorption data should be presented in absolute pressures. Furthermore, BET areas calculated from CO_2 sorption isotherms recorded at 195 K must use a physically reasonable p_0 value. An estimated p_0 for the supercooled liquid phase of CO_2, derived from the phase diagram, is approximately 1.9 bar, almost twice the value of p_0 for the gas-solid transition of CO_2. If a p_0 of 1 bar is incorrectly assumed for analysis at 195 K, the BET surface areas are inaccurately calculated.*

Response. We would like to express our gratitude for your careful review and valuable comments on our work. The following contents have been amended or added in the revised manuscript

The saturation pressure of 191 kPa was used for specific surface area calculation from CO_2 sorption isotherms recorded at 195 K. [34, 35] (Page 18 in the revised manuscript).

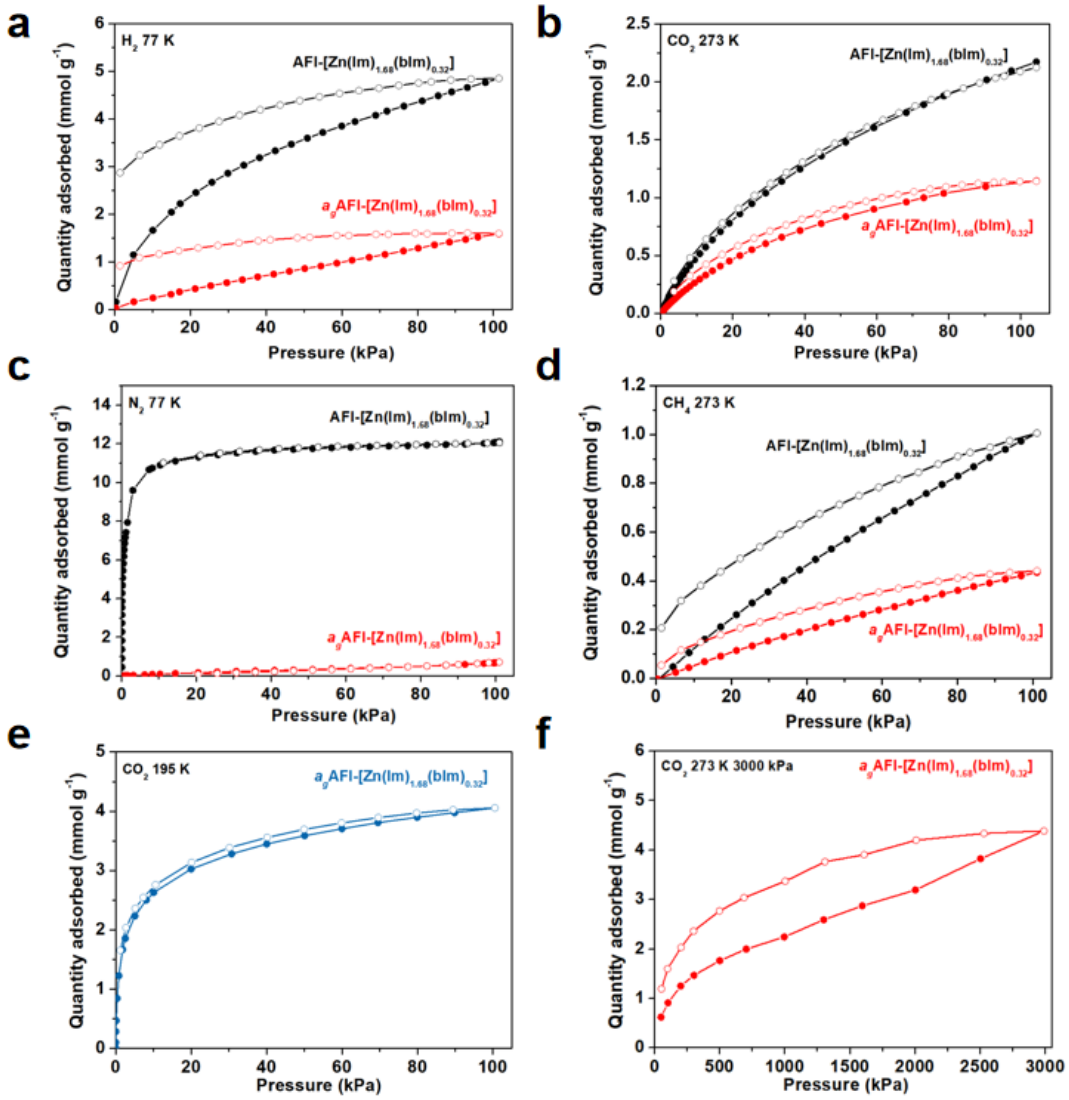

Fig. 4 Gas isotherms of AFI-$[Zn(Im)_{1.68}(bIm)_{0.32}]$ and a_gAFI-$[Zn(Im)_{1.68}(bIm)_{0.32}]$ tested by (a) H_2 at 77 K, (b) CO_2 at 273 K, (c) N_2 at 77 K, (d) CH_4 at 273 K, (e) CO_2 at 195 K, and (f) CO_2 at 273 K up to 3000 kPa.

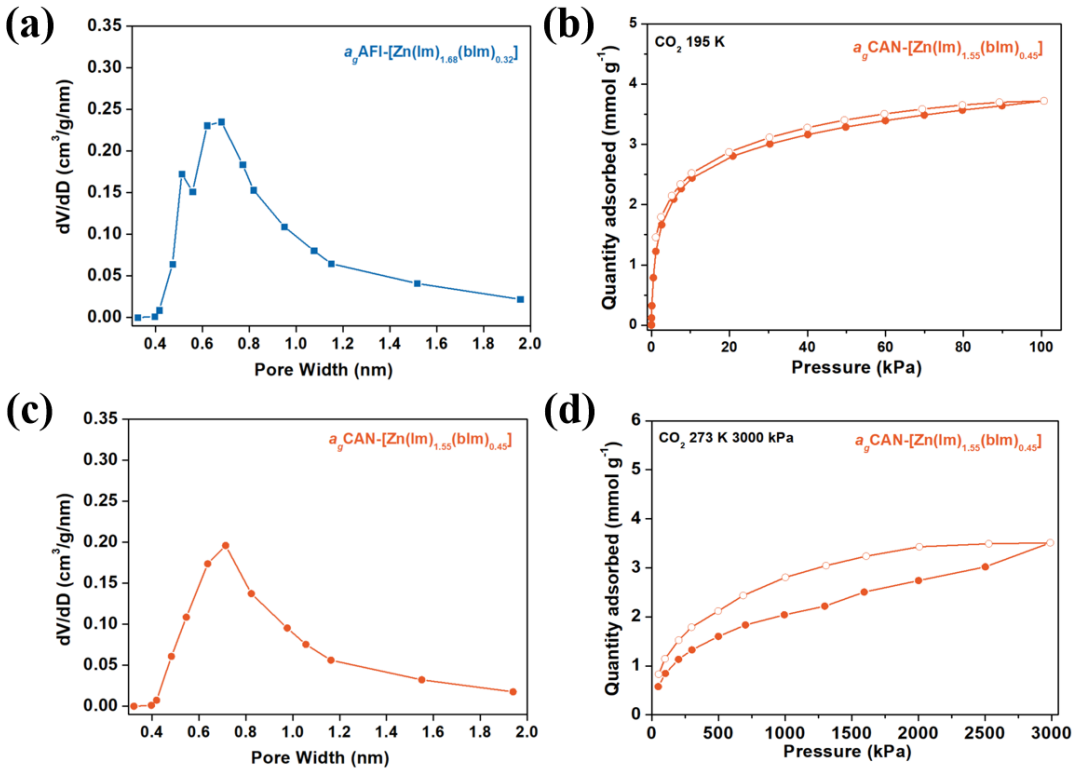

Fig. S19 (a) Pore size distribution of a_gAFI-[Zn(Im)$_{1.68}$(bIm)$_{0.32}$] obtained by CO_2 isotherms at 195 K. (b) CO_2 isotherms at 195 K, (c) pore size distribution, and (d) the high-pressure CO_2 adsorption at 273 K and 3000 kPa for a_gCAN-Zn(Im)$_{1.55}$(bIm)$_{0.45}$].

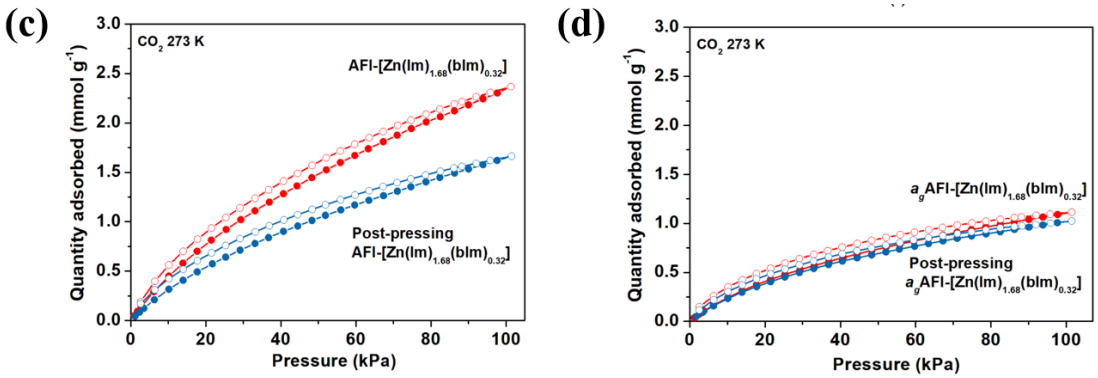

Fig. S20 (c) CO_2 adsorption at 273 K for AFI-[Zn(Im)$_{1.68}$(bIm)$_{0.32}$] and post-pressing AFI-[Zn(Im)$_{1.68}$(bIm)$_{0.32}$], (d) CO_2 adsorption at 273 K for a_gAFI-[Zn(Im)$_{1.68}$(bIm)$_{0.32}$] and post-pressing a_gAFI-[Zn(Im)$_{1.68}$(bIm)$_{0.32}$].

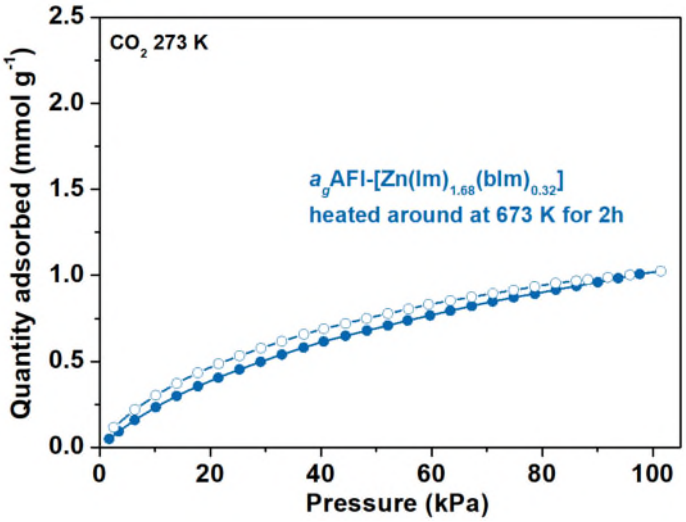

Fig. S21 the CO_2 adsorption isotherm of a_gAFI-$[Zn(Im)_{1.68}(bIm)_{0.32}]_T$ glass heated around at 673 K (above T_g) for 2h.

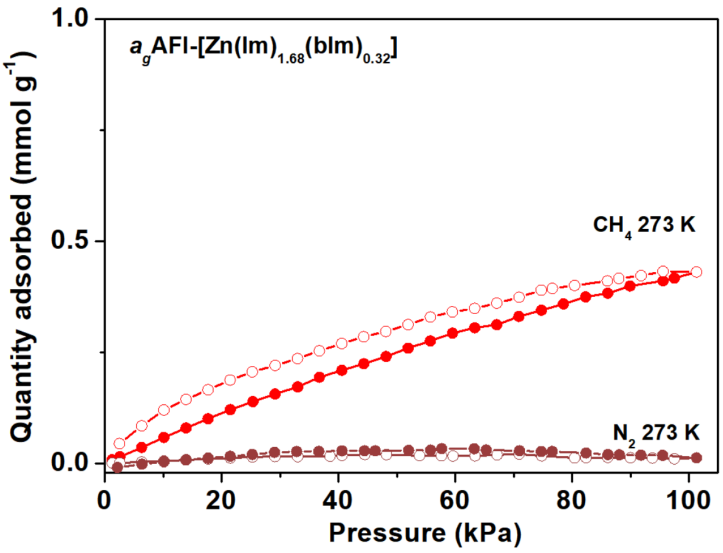

Fig. S24 The CH_4 and N_2 adsorption-desorption curves at 273 K for a_gAFI-$[Zn(Im)_{1.68}(bIm)_{0.32}]$.

[34] Frentzel-Beyme L, et al. Quantification of gas-accessible microporosity in metal-organic framework glasses. *Nat*. *Commun*. **13**, 7750 (2022).

[35] Xue WL, et al. Highly porous metal–organic framework liquids and glasses via a solvent-assisted linker exchange strategy of ZIF–8. *Nat*. *Commun.* **15**, 4420 (2024).

Comments 2. *I previously requested the authors provide estimated standard deviations for their crystallographic data. While this has been done for some of the literature data discussed in the manuscript, the crystallographic parameters extracted from Pawley refinement should also be reported with standard deviations. The software used for profile fitting is not specified (please add this detail), but the package should be capable of providing standard deviations for lattice parameters, which must be included in the supplementary tables.*

Response. Many thanks for your suggestion. The standard deviations for the crystallographic parameters extracted from Pawley refinement, as well as the software used for fitting, have been added in the revised article.

The Pawley refinement was performed using TOPAS (Version 3) program. (Page 17 in the revised manuscript).

Table S2 Lattice parameters of AFI-[$Zn(Im)_2$] and CAN-[$Zn(Im)_2$] obtained from reported cif files and Pawley refinement.

	Space group	**a (Å)**	**b (Å)**	**c (Å)**	**α (º)**	**β (º)**	**γ (º)**	**Ref.**
AFI-[$Zn(Im)_2$]	P6/MCC	26.4372	26.4372	16.6315	90	90	90	Cif
AFI-[$Zn(Im)_2$]	P6/MCC	26.284(7)	26.284(7)	16.243(6)	90	90	90	This work
CAN-[$Zn(Im)_2$]	Pnma	9.6256(8)	23.436(2)	41.593(3)	90	90	90	Cif
CAN-[$Zn(Im)_2$]	Pnma	9.927(4)	19.839(7)	39.00(1)	90	90	90	This work

Table S4 Lattice parameters of MOFs obtained from reported cif files and Pawley refinement.

	Space group	a (Å)	b (Å)	c (Å)	α (°)	β (°)	γ (°)	Ref.
AFI-$[Zn(Im)_2]$	P6/MCC	26.4372	26.4372	16.6315	90	90	90	Cif
AFI-$[Zn(Im)_{1.68}(bIm)_{0.32}]$	P6/MCC	26.137(8)	26.137(8)	16.59(1)	90	90	90	This work
CAN-$[Zn(Im)_2]$	Pnma	9.6256(8)	23.436(2)	41.593(3)	90	90	90	Cif
CAN-$[Zn(Im)_{1.73}(bIm)_{0.27}]$	Pnma	9.623(3)	23.54(1)	41.21(1)	90	90	90	This work

Reviewer #2 (Remarks to the Author):

I have carefully read the revised draft and the attachment, and the manuscript here can be accepted by NC at present.

Response. We thank the reviewer for their in-depth questions and suggestions on our work.

Reviewer #3 (Remarks to the Author):

The authors have fully addressed the concerns, the manuscript in this version can be accepted.

Response. We would like to express our gratitude for your careful review and valuable comments on our work.

Reviewer #4 (Remarks to the Author):

I recommend publishing the manuscript in its current state.

Response. We appreciate the reviewer's comment.